07-09 July 2009

TECH BRIEFS

NATIONAL AERONAUTICS AND SPACE ADMINISTRATION

INTRODUCTION

Tech Briefs are short announcements of innovations originating from research and development activities of the National Aeronautics and Space Administration. They emphasize information considered likely to be transferable across industrial, regional, or disciplinary lines and are issued to encourage commercial application.

Availability of NASA Tech Briefs and TSPs

Requests for individual Tech Briefs or for Technical Support Packages (TSPs) announced herein should be addressed to

National Technology Transfer Center

Telephone No. **(800) 678-6882** or via World Wide Web at **www2.nttc.edu/leads/**

Please reference the control numbers appearing at the end of each Tech Brief. Information on NASA's Innovative Partnerships Program (IPP), its documents, and services is also available at the same facility or on the World Wide Web at **http://ipp.nasa.gov**.

Innovative Partnerships Offices are located at NASA field centers to provide technology-transfer access to industrial users. Inquiries can be made by contacting NASA field centers listed below.

NASA Field Centers and Program Offices

Ames Research Center
Lisa L. Lockyer
(650) 604-1754
lisa.l.lockyer@nasa.gov

Dryden Flight Research Center
Gregory Poteat
(661) 276-3872
greg.poteat@dfrc.nasa.gov

Glenn Research Center
Kathy Needham
(216) 433-2802
kathleen.k.needham@nasa.gov

Goddard Space Flight Center
Nona Cheeks
(301) 286-5810
nona.k.cheeks@nasa.gov

Jet Propulsion Laboratory
Andrew Gray
(818) 354-3821
gray@jpl.nasa.gov

Johnson Space Center
information
(281) 483-3809
jsc.techtran@mail.nasa.gov

Kennedy Space Center
David R. Makufka
(321) 867-6227
david.r.makufka@nasa.gov

Langley Research Center
Brian Beaton
(757) 864-2192
brian.f.beaton@nasa.gov

Marshall Space Flight Center
Jim Dowdy
(256) 544-7604
jim.dowdy@msfc.nasa.gov

Stennis Space Center
Ramona Travis
(228) 688-3832
ramona.e.travis@nasa.gov

Carl Ray, Program Executive
Small Business Innovation Research (SBIR) & Small Business Technology Transfer (STTR) Programs
(202) 358-4652
carl.g.ray@nasa.gov

Doug Comstock, Director
Innovative Partnerships Program Office
(202) 358-2560
doug.comstock@nasa.gov

TECH BRIEFS

NATIONAL AERONAUTICS AND SPACE ADMINISTRATION

Dual Cryogenic Capacitive Density Sensor

John F. Kennedy Space Center, Florida

vA dual cryogenic capacitive density sensor has been developed. The device contains capacitive sensors that monitor two-phase cryogenic flow density to within ±1% accuracy, which, if temperature were known, could be used to determine the ratio of liquid to gas in the line. Two of these density sensors, located a known distance apart, comprise the sensor, providing some information on the velocity of the flow.

This sensor was constructed as a proposed mass flowmeter with high data acquisition rates. Without moving parts, this device is capable of detecting the density change within a two-phase cryogenic flow more than 100 times a second. Detection is enabled by a series of two sets of five parallel plates with stainless steel, cryogenically rated tubing. The parallel plates form the two capacitive sensors, which are measured by electrically isolated digital electronics. These capacitors monitor the dielectric of the flow — essentially the density of the flow — and can be used to determine (along with temperature) the ratio of cryogenic liquid to gas. Combining this information with the velocity of the flow can, with care, be used to approximate the total two-phase mass flow.

The sensor can be operated at moderately high pressures and can be lowered into a cryogenic bath. The electronics have been substantially improved over the older sensors, incorporating a better microprocessor, elaborate ground loop protection and noise limiting circuitry, and reduced temperature sensitivity. At the time of this writing, this design has been bench tested at room temperature, but actual cryogenic tests are pending

This work was done by Robert Youngquist of Kennedy Space Center and Carlos Mata, Peter Vokrot, and Robert Cox of ASRC Aerospace Corporation. Further information is contained in a TSP (see page 1). ***KSC-13058***

Hail Monitor Sensor

This method of hail monitoring would be useful for the military and the commercial airline industry.

John F. Kennedy Space Center, Florida

Figure 1 shows damage to the space shuttle's external tank (ET) that was likely caused by a pea-sized hailstone. Because of the potential damage to the ET while exposed to the weather, it is important to remotely monitor the hail fall in the vicinity of the shuttle pad. If hail of sufficient size and quantity is detected by a hail-monitoring system, the ET would be subsequently thoroughly inspected for damage.

An inexpensive and simple hail monitor design has been developed that has a single piezoelectric ceramic disc and uses a metal plate as a sounding board. The structure is durable and able to withstand the launch environment. This design has several advantages over a multi-ceramic sensor, including reduced cost and complexity, increased durability, and improvement in impact response uniformity over the active surface. However, the most important characteristic of this design is the potential to use frequency discrimination between the spectrum created from raindrop impact and a hailstone impact. The sound of hail hitting a metal plate is distinctly different from the sound of rain hitting the same plate.

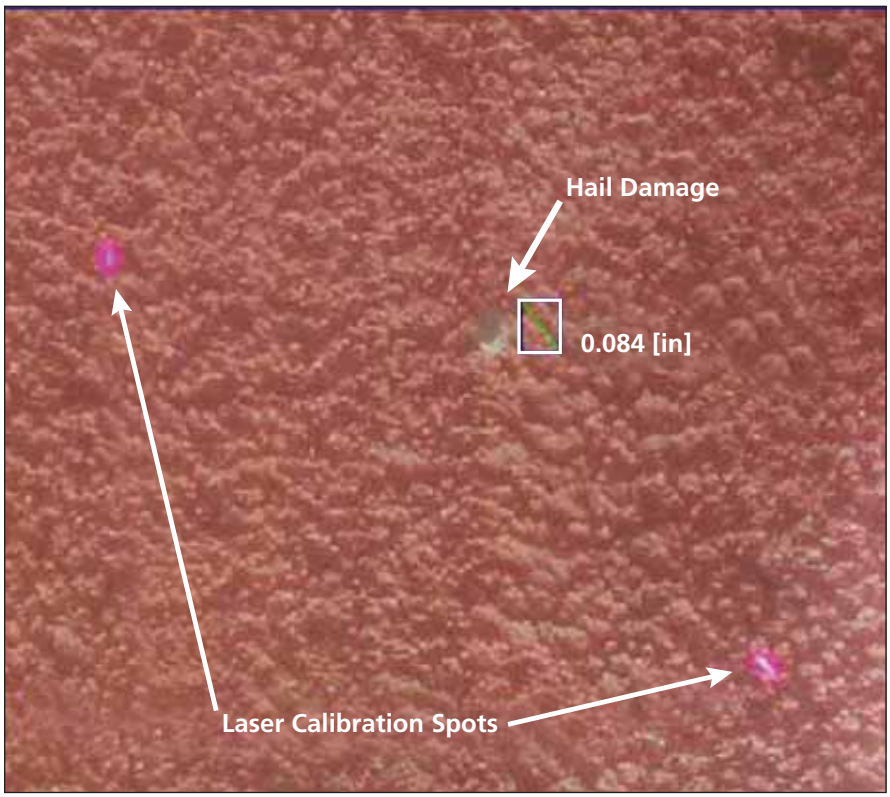

Figure 1. This **Example of Hail Damage** on the surface of the shuttle's external tank likely was caused by a pea-sized hailstone.

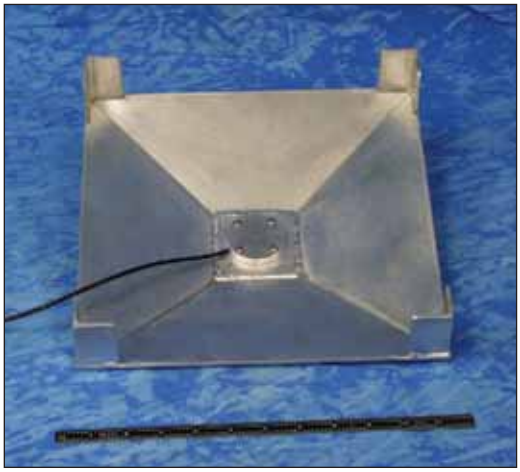

Figure 2. The prototype of the **Hall Monitor Sensor** uses a single piezoelectric ceramic disc with a metal plate as a sounding board. The concept was improved by forming a shallow pyramid structure so that hail would bounce away from the sensor and not be counted more than once.

This fortuitous behavior of the pyramid sensor may lead to a signal processing strategy, which is inherently more reliable than one depending on amplitude processing only.

The initial concept has been improved by forming a shallow pyramid structure so that hail is encouraged to bounce away from the sensor so as not to be counted more than once. The sloped surface also discourages water from collecting. Additionally, the final prototype version includes a mounting box for the piezo-ceramic, which is offset from the pyramid apex, thus helping to reduce non-uniform response (see Figure 2).

The frequency spectra from a single raindrop impact and a single ice ball impact have been compared. The most notable feature of the frequency resonant peaks is the ratio of the 5.2 kHz to 3.1 kHz components. In the case of a raindrop, this ratio is very small. But in the case of an ice ball, the ratio is roughly one third. This frequency signature of ice balls should provide a robust method for discriminating raindrops from hailstones.

Considering that hail size distributions (HSDs) and fall rates are roughly 1 percent that of rainfall, hailstone sizes range from a few tenths of a centimeter to several centimeters. There may be considerable size overlap between large rain and small hail. As hail occurs infrequently at KSC, the ideal HSD measurement sensor needs to have a collection area roughly 100 times greater than a raindrop-size distribution sensor or disdrometer. The sensitivity should be such that it can detect and count very small hail in the midst of intense rainfall consisting of large raindrop sizes. The dynamic range and durability should allow measurement of the largest hail sizes, and the operation and calibration strategy should consider the infrequent occurrence of hail fall over the KSC area.

This work was done by Robert Youngquist of Kennedy Space Center; William Haskell of Sierra Lobo, Inc.; and Christopher Immer, Bobby Cox, and John Lane of ASRC Aerospace. Further information is contained in a TSP (see page 1). ***KSC-12594***

Miniature Six-Axis Load Sensor for Robotic Fingertip

Lyndon B. Johnson Space Center, Houston, Texas

A miniature load sensor has been developed as a prototype of tactile sensors that could fit within fingertips of anthropomorphic robot hands. The sensor includes a force-and-torque transducer in the form of a spring instrumented with at least six semiconductor strain gauges. The strain-gauge wires are secured to one side of an interface circuit board mounted at the base of the spring. This board protects the strain-gauge wires from damage that could otherwise occur as a result of finger motions.

On the opposite side of the interface board, cables routed along the neutral axis of the finger route the strain-gauge output voltages to an analog-to-digital converter (A/D) board. The A/D board is mounted as close as possible to the strain gauges to minimize electromagnetic noise and other interference effects. The outputs of the A/D board are fed to a controller, wherein, by means of a predetermined calibration matrix, the digitized strain-gauge output voltages are converted to three vector components of force and three of torque exerted by or on the fingertip.

This work was done by Myron A. Diftler and Toby B. Martin of Johnson Space Center, Michael C. Valvo and Dagoberto Rodriguez of Lockheed Martin Corp., and Mars W. Chu of Metrica, Inc. Further information is contained in a TSP (see page 1). ***MSC-23910-1***

Improved Blackbody Temperature Sensors for a Vacuum Furnace

Through proper selection of materials, it is possible to satisfy severe requirements.

Marshall Space Flight Center, Alabama

Some improvements have been made in the design and fabrication of blackbody sensors (BBSs) used to measure the temperature of a heater core in a vacuum furnace. Each BBS consists of a ring of thermally conductive, high-melting-temperature material with two tantalum-sheathed thermocouples attached at diametrically opposite points. The name "blackbody sensor" reflects the basic principle of operation. Heat is transferred between the ring and the furnace heater core primarily by blackbody radiation, heat is conducted through the ring to the thermocouples, and the temperature of the ring (and, hence, the temperature of the heater core) is measured by use of the thermocouples.

Two main requirements have guided the development of these BBSs: (1) The rings should have as high an emissivity as possible in order to maximize the heat-transfer rate and thereby maximize temperature-monitoring performance and (2) the thermocouples must be joined to the rings in such a way as to ensure long-term, reliable intimate thermal contact. The problem of fabricating a BBS to satisfy these requirements is complicated by an application-specific prohibi-

tion against overheating and thereby damaging nearby instrumentation leads through the use of conventional furnace brazing or any other technique that involves heating the entire BBS and its surroundings. The problem is further complicated by another application-specific prohibition against damaging the thin tantalum thermocouple sheaths through the use of conventional welding to join the thermocouples to the ring.

The first BBS rings were made of graphite. The tantalum-sheathed thermocouples were attached to the graphite rings by use of high-temperature graphite cements. The ring/thermocouple bonds thus formed were found to be weak and unreliable, and so graphite rings and graphite cements were abandoned.

Now, each BBS ring is made from one of two materials: either tantalum or a molybdenum/titanium/zirconium alloy. The tantalum-sheathed thermocouples are bonded to the ring by laser brazing. The primary advantage of laser brazing over furnace brazing is that in laser brazing, it is possible to form a brazed connection locally, without heating nearby parts to the flow temperature of the brazing material. Hence, it is possible to comply with the prohibition against overheating nearby instrumentation leads. Also, in laser brazing, unlike in furnace brazing, it is possible to exert control over the thermal energy to such a high degree that it becomes possible to braze the thermocouples to the ring without burning through the thin tantalum sheaths on the thermocouples.

The brazing material used in the laser brazing process is a titanium-boron paste. This brazing material can withstand use at temperatures up to about 1,400°C. In thermal-cycling tests performed thus far, no debonding between the rings and thermocouples has been observed. Emissivity coatings about 0.001 in. (≈0.025 mm) thick applied to the interior surfaces of the rings have been found to improve the performance of the BBS sensors by raising the apparent emissivities of the rings. In thermal-cycling tests, the coatings were found to adhere well to the rings.

This work was done by Jeff Farmer and Chris Coppens of Marshall Space Flight Center and J. Scott O'Dell, Timothy N. McKechnie, and Elizabeth Schofield of Plasma Processes Inc. For further information, contact Sammy Nabors, MSFC Commercialization Assistance Lead, at sammy.a.nabors@nasa.gov. Refer to MFS-32095-1.

Wrap-Around Out-the-Window Sensor Fusion System

Lyndon B. Johnson Space Center, Houston, Texas

The Advanced Cockpit Evaluation System (ACES) includes communication, computing, and display subsystems, mounted in a van, that synthesize out-the-window views to approximate the views of the outside world as it would be seen from the cockpit of a crewed spacecraft, aircraft, or remote control of a ground vehicle or UAV (unmanned aerial vehicle). The system includes five flat-panel display units arranged approximately in a semicircle around an operator, like cockpit windows. The scene displayed on each panel represents the view through the corresponding cockpit window. Each display unit is driven by a personal computer equipped with a video-capture card that accepts live input from any of a variety of sensors (typically, visible and/or infrared video cameras).

Software running in the computers blends the live video images with synthetic images that could be generated, for example, from heads-up-display outputs, waypoints, corridors, or from satellite photographs of the same geographic region. Data from a Global Positioning System receiver and an inertial navigation system aboard the remote vehicle are used by the ACES software to keep the synthetic and live views in registration. If the live image were to fail, the synthetic scenes could still be displayed to maintain situational awareness.

This work was done by Jeffrey Fox, Eric A. Boe, and Francisco Delgado of Johnson Space Center; James B. Secor II of Barrios Technology, Inc.; Michael R. Clark and Kevin D. Ehlinger of Jacobs Sverdrup; and Michael F. Abernathy of Rapid Imaging Software, Inc. Further information is contained in a TSP (see page 1).

Rapid Imaging Software, Inc. has requested permission to assert copyright for the software code. MSC-24020-1

Wide-Range Temperature Sensors With High-Level Pulse Train Output

John H. Glenn Research Center, Cleveland, Ohio

Two types of temperature sensors have been developed for wide-range temperature applications. The two sensors measure temperature in the range of –190 to +200 °C and utilize a thin-film platinum RTD (resistance temperature detector) as the temperature-sensing element. Other parts used in the fabrication of these sensors include NPO (negative-positive-zero) type ceramic capacitors for timing, thermally-stable film or wire-wound resistors, and high-temperature circuit boards and solder.

The first type of temperature sensor is a relaxation oscillator circuit using an SOI (silicon-on-insulator) operational amplifier as a comparator. The output is a pulse train with a period that is roughly proportional to the temperature being measured. The voltage level of the pulse train is high-level, for example 10 V. The high-level output makes the sensor less sensitive to noise or electromagnetic interference. The output can be read by a frequency or period meter and then converted into a temperature reading.

The second type of temperature sensor is made up of various types of multivibrator circuits using an SOI type 555 timer and the passive components mentioned above. Three configurations have been developed that were

based on the technique of charging and discharging a capacitor through a resistive element to create a train of pulses governed by the capacitor-resistor time constant.

Both types of sensors, which operated successfully over the wide temperature range, have potential use in extreme temperature environments including jet engines and space exploration missions.

This work was done by Richard L. Patterson of Glenn Research Center and Ahmad Hammoud of ASRC Aerospace Corp. Further information is contained in a TSP (see page 1). ***Inquiries concerning rights for the commercial use of this invention should be addressed to NASA Glenn Research Center, Innovative Partnerships Office, Attn: Steve Fedor, Mail Stop 4–8, 21000 Brookpark Road, Cleveland, Ohio 44135. Refer to LEW-18350-1.***

Terminal Descent Sensor Simulation

NASA's Jet Propulsion Laboratory, Pasadena, California

Sulcata software simulates the operation of the Mars Science Laboratory (MSL) radar terminal descent sensor (TDS). The program models TDS radar antennas, RF hardware, and digital processing, as well as the physics of scattering from a coherent ground surface. This application is specific to this sensor and is flexible enough to handle end-to-end design validation. Sulcata is a high-fidelity simulation and is used for performance evaluation, anomaly resolution, and design validation.

Within the trajectory frame, almost all internal vectors are represented in whatever coordinate system is used to represent platform position. The trajectory frame must be planet-fixed. The platform body frame is specified relative to arbitrary reference points relative to the platform (spacecraft or test vehicle). Its rotation is a function of time from the trajectory coordinate system specified via dynamics input (file for open loop, callback for closed loop). Orientation of the frame relative to the body is arbitrary, but constant over time.

The TDS frame must have a constant rotation and translation from the platform body frame specified at run time. The DEM frame has an arbitrary, but time-constant, rotation and translation with respect to the simulation frame specified at run time. It has the same orientation as sigma0 frame, but is possibly translated. Surface sigma0 has the same arbitrary rotation and translation as DEM frame.

This work was done by Curtis W. Chen of Caltech for NASA's Jet Propulsion Laboratory. Further information is contained in a TSP (see page 1).

This software is available for commercial licensing. Please contact Karina Edmonds of the California Institute of Technology at (626) 395-2322. Refer to NPO-46161.

A Robust Mechanical Sensing System for Unmanned Sea Surface Vehicles

NASA's Jet Propulsion Laboratory, Pasadena, California

The need for autonomous navigation and intelligent control of unmanned sea surface vehicles requires a mechanically robust sensing architecture that is watertight, durable, and insensitive to vibration and shock loading. The sensing system developed here comprises four black and white cameras and a single color camera. The cameras are rigidly mounted to a camera bar that can be reconfigured to mount multiple vehicles, and act as both navigational cameras and application cameras. The cameras are housed in watertight casings to protect them and their electronics from moisture and wave splashes.

Two of the black and white cameras are positioned to provide lateral vision. They are angled away from the front of the vehicle at horizontal angles to provide ideal fields of view for mapping and autonomous navigation. The other two black and white cameras are positioned at an angle into the color camera's field of view to support vehicle applications. These two cameras provide an overlap, as well as a backup to the front camera. The color camera is positioned directly in the middle of the bar, aimed straight ahead. This system is applicable to any sea-going vehicle, both on Earth and in space.

This work was done by Eric A. Kulczycki, Lee J. Magnone, Terrance Huntsberger, Hrand Aghazarian, Curtis W. Padgett, David C. Trotz, and Michael S. Garrett of Caltech for NASA's Jet Propulsion Laboratory. For more information, contact iaoffice@jpl.nasa.gov.
NPO-46372

Additive for Low-Temperature Operation of Li-$(CF)_n$ Cells

Tris(2,2,2-trifluoroethyl) borate as an electrolyte additive increases low-temperature capacity.

NASA's Jet Propulsion Laboratory, Pasadena, California

Some progress has been reported in continuing research on the use of anion-receptor compounds as electrolyte additives to increase the sustainable rates of discharge and, hence, the discharge capacities, of lithium-poly(carbon monofluoride) [Li-$(CF)_n$, where n >1] primary electrochemical power cells. Some results of this research at a prior stage were summarized in "Increasing Discharge Capacities of Li$(CF)_n$ Cells" (NPO-42346), *NASA Tech Briefs*, Vol. 32, No. 2 (February 2008), page 37. A major difference between the present and previously reported results is that now there is some additional focus on improving performance at temperatures from ambient down to as low as –40 °C.

To recapitulate from the cited prior article: During the discharge of a Li-$(CF)_n$ cell, one of the electrochemical reactions causes LiF to precipitate at the cathode. LiF is almost completely insoluble in most non-aqueous solvents, including those used in the electrolyte solutions of Li-$(CF)_n$ cells. LiF is electrochemically inactive and can block the desired transport of electrons at the cathode, and, hence, the precipitation of LiF can form an ever-thickening film on the cathode that limits the rate of discharge. An anion-receptor electrolyte additive helps to increase the discharge capacity in two ways:

- It renders LiF somewhat soluble in the non-aqueous electrolyte solution, thereby delaying precipitation until a high concentration of LiF in solution has been reached.
- When precipitation occurs, it promotes the formation of large LiF grains that do not conformally coat the cathode.

The net effect is to reduce the blockage caused by precipitation of LiF, thereby maintaining a greater degree of access of electrolyte to the cathode and greater electronic conductivity.

The anion-receptor compounds studied in this line of research have been fluorinated boron-based compounds. The specific compound mentioned in the cited prior article, in which there was no special focus on low-temperature performance, was tris(hexafluoroisopropyl) borate. The anion-receptor compound used in the more-recent research reported here — tris(2,2,2-trifluoroethyl) borate — was selected because of an expectation that it would reduce the viscosity of the electrolyte, thereby increasing the low-temperature conductivity and, consequently, increasing the low-temperature discharge-rate capability. One complicating observation made in this research was that tris(2,2,2-trifluoroethyl) borate does not improve the low-temperature performance of a cell containing a fully fluorinated $(CF)_n$ cathode, but does improve the low-temperature performance of a cell containing a sub-fluorinated $(CF)_n$ cathode — that is, a cathode made of $(CF_x)_n$ [where x<1].

The improvement in low-temperature performance can be considerable. For example, in one set of tests at a temperature of –40 °C, a pair of cells that did not contain the present anion-receptor additive and another pair of cells that did contain this additive were discharged at a current of $C/2.5$ (where C is the magnitude of the current, integrated for one hour, that would amount to the nominal charge capacity of a cell). The results of the tests (see figure) showed that the cells containing the additive performed much better than did the cells without the additive.

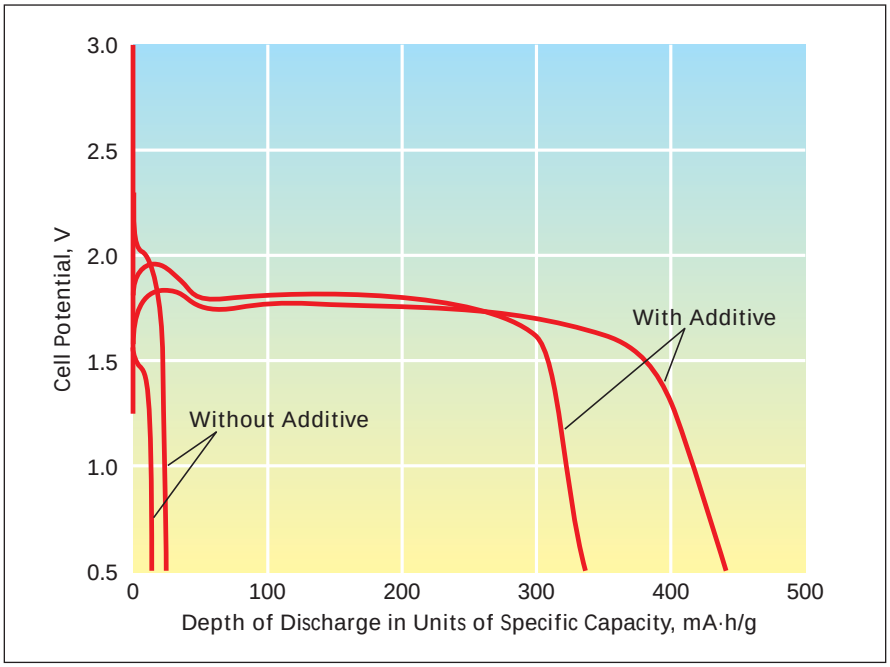

Two Pairs of Li-$(CF_x)_n$ Cells containing an electrolyte in the form of 0.5 M $LiBF_4$ in a non-aqueous solvent were discharged at a rate $C/2.5$ at a temperature of –40 °C. The cells not containing the electrolyte additive were essentially nonfunctional; those containing the additive were functional, retaining approximately half of their room-temperature discharge capacities.

This work was done by William West and Jay Whitacre of Caltech for NASA's Jet Propulsion Laboratory. Further information is contained in a TSP (see page 1).

In accordance with Public Law 96-517, the contractor has elected to retain title to this invention. Inquiries concerning rights for its commercial use should be addressed to:

Innovative Technology Assets Management
JPL
Mail Stop 202-233
4800 Oak Grove Drive
Pasadena, CA 91109-8099
(818) 354-2240
E-mail: iaoffice@jpl.nasa.gov

Refer to NPO-43579, volume and number of this NASA Tech Briefs *issue, and the page number.*

Li/CF_X Cells Optimized for Low-Temperature Operation

Several prior developments are combined.

NASA's Jet Propulsion Laboratory, Pasadena, California

Some developments reported in prior *NASA Tech Briefs* articles on primary electrochemical power cells containing lithium anodes and fluorinated carbonaceous (CF_x) cathodes have been combined to yield a product line of cells optimized for relatively-high-current operation at low temperatures at which commercial lithium-based cells become useless. These developments have involved modifications of the chemistry of commercial Li/CF_x cells and batteries, which are not suitable for high-current and low-temperature applications because they are current-limited and their maximum discharge rates decrease with decreasing temperature.

One of two developments that constitute the present combination is, itself, a combination of developments: (1) the use of sub-fluorinated carbonaceous (CF_x wherein x<1) cathode material, (2) making the cathodes thinner than in most commercial units, and (3) using non-aqueous electrolytes formulated especially to enhance low-temperature performance. This combination of developments was described in more detail in "High-Energy-Density, Low-Temperature Li/CF_x Primary Cells" (NPO-43219), *NASA Tech Briefs*, Vol. 31, No. 7 (July 2007), page 43. The other development included in the present combination is the use of an anion receptor as an electrolyte additive, as described in the immediately preceding article, "Additive for Low-Temperature Operation of Li-$(CF)_n$ Cells" (NPO-43579).

A typical cell according to the present combination of developments contains an anion-receptor additive solvated in an electrolyte that comprises $LiBF_4$ dissolved at a concentration of 0.5 M in a mixture of four volume parts of 1,2 dimethoxyethane with one volume part of propylene carbonate. The proportion, x, of fluorine in the cathode in such a cell lies between 0.5 and 0.9. The best of such cells fabricated to date have exhibited discharge capacities as large as 0.6 A·h per gram at a temperature of –50 °C when discharged at a rate of $C/5$ (where C is the magnitude of the current, integrated for one hour, that would amount to the nominal charge capacity of a cell).

This work was done by William West, Marshall Smart, Jay Whitacre, Ratnakumar Bugga, and Rachid Yazami of Caltech for NASA's Jet Propulsion Laboratory.

In accordance with Public Law 96-517, the contractor has elected to retain title to this invention. Inquiries concerning rights for its commercial use should be addressed to:

Innovative Technology Assets Management
JPL
Mail Stop 202-233
4800 Oak Grove Drive
Pasadena, CA 91109-8099
(818) 354-2240
E-mail: iaoffice@jpl.nasa.gov

Refer to NPO-43585, volume and number of this NASA Tech Briefs *issue, and the page number.*

Number Codes Readable by Magnetic-Field-Response Recorders

Where useable, these codes offer advantages over conventional optical bar codes.

Langley Research Center, Hampton, Virginia

A method of encoding and reading numbers incorporates some of the features of conventional optical bar coding and radio-frequency identification (RFID) tagging, but overcomes some of the disadvantages of both: (1) Unlike in conventional optical bar coding, numbers can be read without having a line of sight to a tag; and (2) the tag circuitry is simpler than the circuitry used in conventional RFID.

The method is based largely on the principles described in "Magnetic-Field-Response Measurement-Acquisition System" (LAR-16908), *NASA Tech Briefs*, Vol. 30, No. 6 (June 2006) page 28. To recapitulate: A noncontact system includes a monitoring unit that acquires measurements from sensors at distances of the order of several meters. Each sensor is a passive radio-frequency (RF) resonant circuit in the form of one or more inductor(s) and capacitor(s). The monitoring unit — a handheld unit denoted a magnetic field response recorder (MFRR) — generates an RF magnetic field that excites oscillations in the resonant circuits resulting in the sensors responding with their own radiated magnetic field. The resonance frequency of each sensor is made to differ significantly from that of the other sensors to facilitate distinction among the responses of different sensors. The MFRR measures selected aspects of the sensor responses: in a typical application, the sensors are designed so that their resonance frequencies vary somewhat with the sensed physical quantities and, accordingly, the MFRR measures the resonance frequencies and variations thereof as indications of those quantities.

In the present method, the resonance circuits are not used as sensors. Instead, the circuits are made to resonate at fixed frequencies that correspond to digits to be encoded. The number-encoding scheme is best explained by means of examples in which each resonant circuit consists of a spiral trace inductor electrically connected to a set of parallel-connected capacitors in the form of interdigitated electrode pairs (see figure). The inductor and capacitor(s) in each resonant circuit can be fabricated as a patterned thin metal film by means of established metal-deposition and -patterning techniques. The capacitance and, hence, the resonance frequency, depends on the number of interdigitated electrodes connected to the inductor. In a similar manner, sets of electrodes could be used.

Initially, in each resonant circuit as fabricated, the number (N) of interdigitated electrode pairs equals the base (e.g., 10) of the number system of the

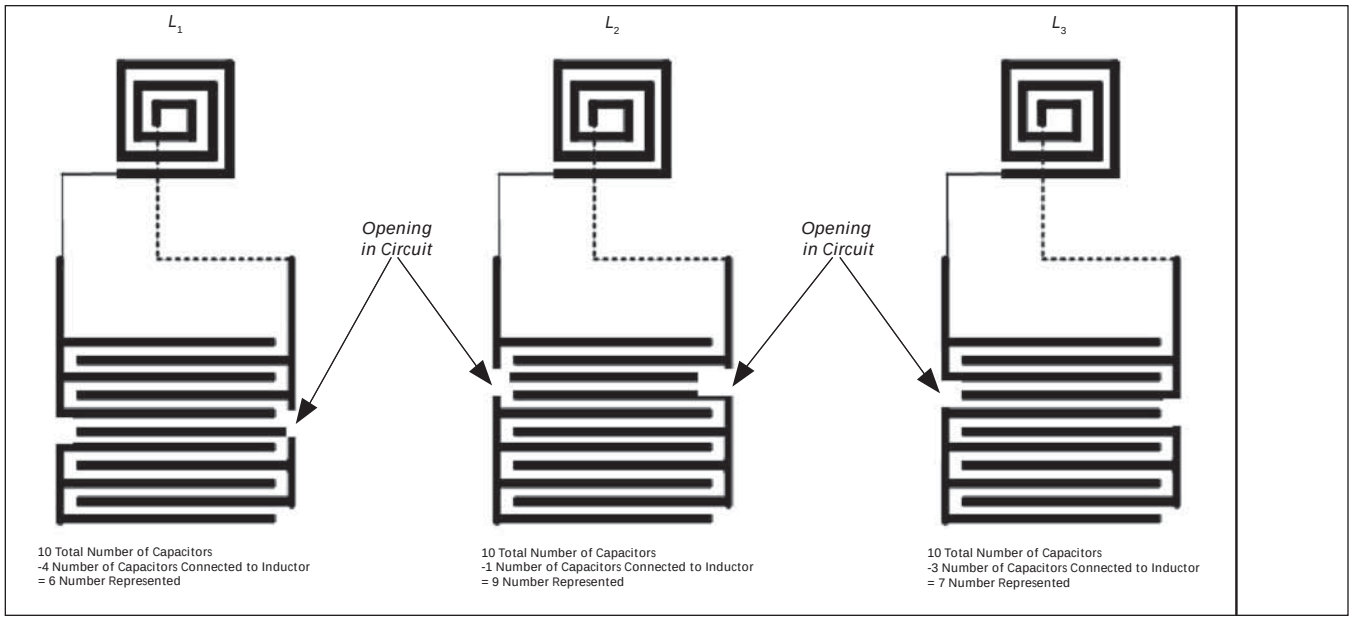

Three Resonant Circuits contain interdigitated-electrode capacitors that can be trimmed to encode digits between 0 to 9. In this case, they have been trimmed to encode the number 697.

digit to be represented by that circuit. *N* electrode pairs represent the digit 0 with the corresponding resonance frequency having the lowest assigned value. To encode a given nonzero digit (*m*), one punches a hole or makes a cut in the electrode pattern so as to disconnect *m* of the electrode pairs (or, sets of electrode pairs) from the inductor, reducing the capacitance and thereby increasing the resonance frequency to a value assigned to represent the digit *m*. The resulting frequency, ω_m, becomes (the capacitance for each electrode pair or set of electrode pairs is *C*)

$$\omega_m = \frac{1}{2\pi\sqrt{(N-m)L_iC}}$$

In the example shown at the left side of the figure, to encode the digit 6, one disconnects the electrodes of the lowermost 6 of 10 electrode pairs. If there is a need to encode more than one digit (e.g., three digits as in the figure), then one can fabricate the corresponding number of resonant circuits having the same capacitor arrangement but having inductance values (L_1, L_2, L_3) that differ sufficiently so that their resonance-frequency ranges do not overlap.

This method offers the following advantages in addition to the ones mentioned above:

- A number can be read, irrespective of the orientation of a tag containing the resonant circuits that encode the number.
- Numbers can be read at distances greater than the maximum reading distances of optical bar-code readers.
- A tag can be embedded or enclosed in electrically nonconductive material.
- A tag is secure in the sense that once it is embedded or enclosed in a protective material, there is no way to alter the encoded number in normal use.
- The method cannot store or acquire information providing ease of mind to consumers when used in retail.

This work was done by Stanley E. Woodard of NASA Langley Research Center and Bryant D. Taylor of Swales Aerospace for Langley Research Center. Further information is contained in a TSP (see page 1). ***LAR-16483-1***

Determining Locations by Use of Networks of Passive Beacons

This method could be an alternative to GPS in some situations.

NASA's Jet Propulsion Laboratory, Pasadena, California

Networks of passive radio beacons spanning moderate-sized terrain areas have been proposed to aid navigation of small robotic aircraft that would be used to explore Saturn's moon Titan. Such networks could also be used on Earth to aid navigation of robotic aircraft, land vehicles, or vessels engaged in exploration or reconnaissance in situations or locations (e.g., underwater locations) in which Global Positioning System (GPS) signals are unreliable or unavailable.

Prior to use, it would be necessary to pre-position the beacons at known locations that would be determined by use of one or more precise independent global navigation system(s). Thereafter, while navigating over the area spanned by a given network of passive beacons, an exploratory robot would use the beacons to determine its position precisely relative to the known beacon positions (see figure). If it were necessary for the robot to explore multiple, separated terrain areas spanned by different networks of beacons, the robot could use a long-haul, relatively coarse global navigation system for the lower-precision position determination needed during transit between such areas.

The proposed method of precise determination of position of an exploratory robot relative to the positions of passive radio beacons is based partly on the principles of radar and partly on the principles of radio-frequency identi-

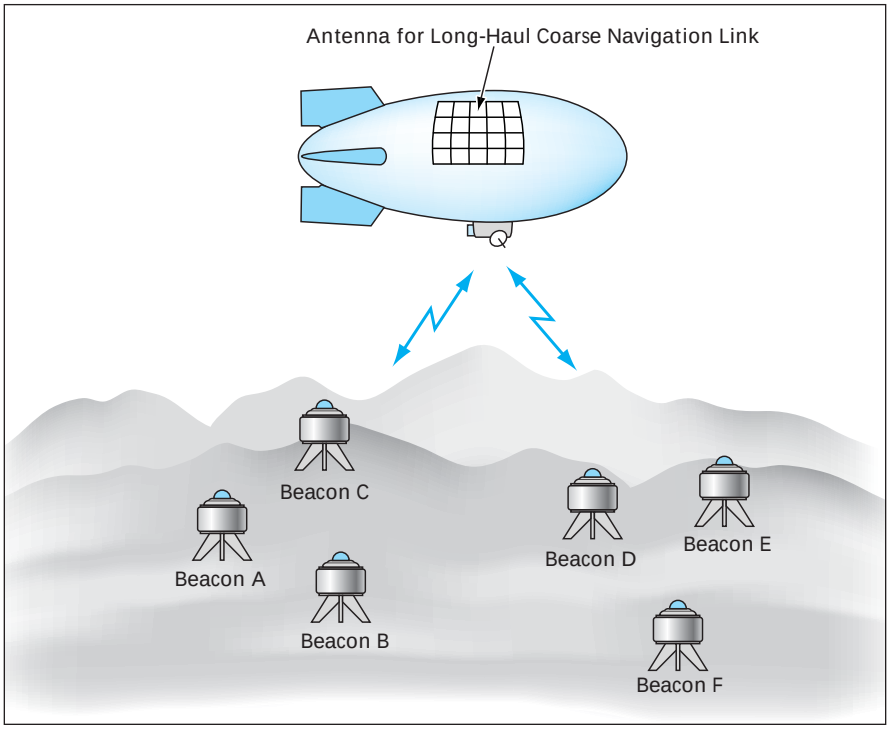

A **Robotic Exploratory Aircraft** (e.g., a miniature blimp) would transmit a radarlike signal to interrogate passive radio beacons on the ground. The navigation system of the aircraft would store the known locations of the beacons and would utilize the signals returning from the beacons to determine its precise position relative to the network of beacons. The navigation system would also synthesize a navigation map from a combination of the stored beacon location data and from prior and present coarse and fine position estimates.

fication (RFID) tags. The robot would transmit radarlike signals that would be modified and reflected by the passive beacons. The distance to each beacon would be determined from the round-trip propagation time and/or round-trip phase shift of the signal returning from that beacon. Signals returned from different beacons could be distinguished by means of their RFID characteristics. Alternatively or in addition, the antenna of each beacon could be designed to radiate in a unique pattern that could be identified by the navigation system. Also, alternatively or in addition, sets of identical beacons could be deployed in unique configurations such that the navigation system could identify their unique combinations of radio-frequency reflections as an alternative to leveraging the uniqueness of the RFID tags.

The degree of dimensional accuracy would depend not only on the locations of the beacons but also on the number of beacon signals received, the number of samples of each signal, the motion of the robot, and the time intervals between samples. At one extreme, a single sample of the return signal from a single beacon could be used to determine the distance from that beacon and hence to determine that the robot is located somewhere on a sphere, the radius of which equals that distance and the center of which lies at the beacon. In a less extreme example, the three-dimensional position of the robot could be determined with fair precision from a single sample of the signal from each of three beacons. In intermediate cases, position estimates could be refined and/or position ambiguities could be resolved by use of supplementary readings of an altimeter and other instruments aboard the robot.

This work was done by Clayton Okino, Andrew Gray, and Esther Jennings of Caltech for NASA's Jet Propulsion Laboratory. For more information, contact iaoffice@jpl.nasa.gov.
NPO-40042

Superconducting Hot-Electron Submillimeter-Wave Detector

Sensitivity and speed are increased beyond those of related prior devices.

NASA's Jet Propulsion Laboratory, Pasadena, California

A superconducting hot-electron bolometer has been built and tested as a prototype of high-sensitivity, rapid-response detectors of submillimeter-wavelength radiation. There are diverse potential applications for such detectors, a few examples being submillimeter spectroscopy for scientific research; detection of leaking gases; detection of explosive, chemical, and biological weapons; and medical imaging.

This detector is a superconducting-transition-edge device. Like other such devices, it includes a superconducting bridge that has a low heat capacity and is maintained at a critical temperature (T_c) at the lower end of its superconducting-transition temperature range. Incident photons cause transient increases in electron temperature through the superconducting-transition range, thereby yielding measurable increases in electrical resistance. In this case, T_c = 6 K, which is approximately the upper limit of the operating-temperature range of silicon-based bolometers heretofore used routinely in many laboratories. However, whereas the response speed of a typical silicon-based laboratory bolometer is characterized by a frequency of the order of a kilohertz, the response speed of the present device is much higher — characterized by a frequency of the order of 100 MHz.

For this or any bolometer, a useful figure of merit that one seeks to minimize is $(\mathrm{NEP})\tau^{1/2}$, where NEP denotes the noise-equivalent power (NEP) and τ the response time. This figure of merit depends primarily on the heat capacity and, for a given heat capacity, is approximately invariant. As a consequence of this approximate invariance, in designing a device having a given heat capacity to be more sensitive (to have lower NEP), one must accept longer response time (slower response) or, conversely, in designing it to respond faster, one must accept lower sensitivity. Hence, further, in order to increase both the speed of response and the sensitivity, one must make the device very small in order to make its heat capacity very small; this is

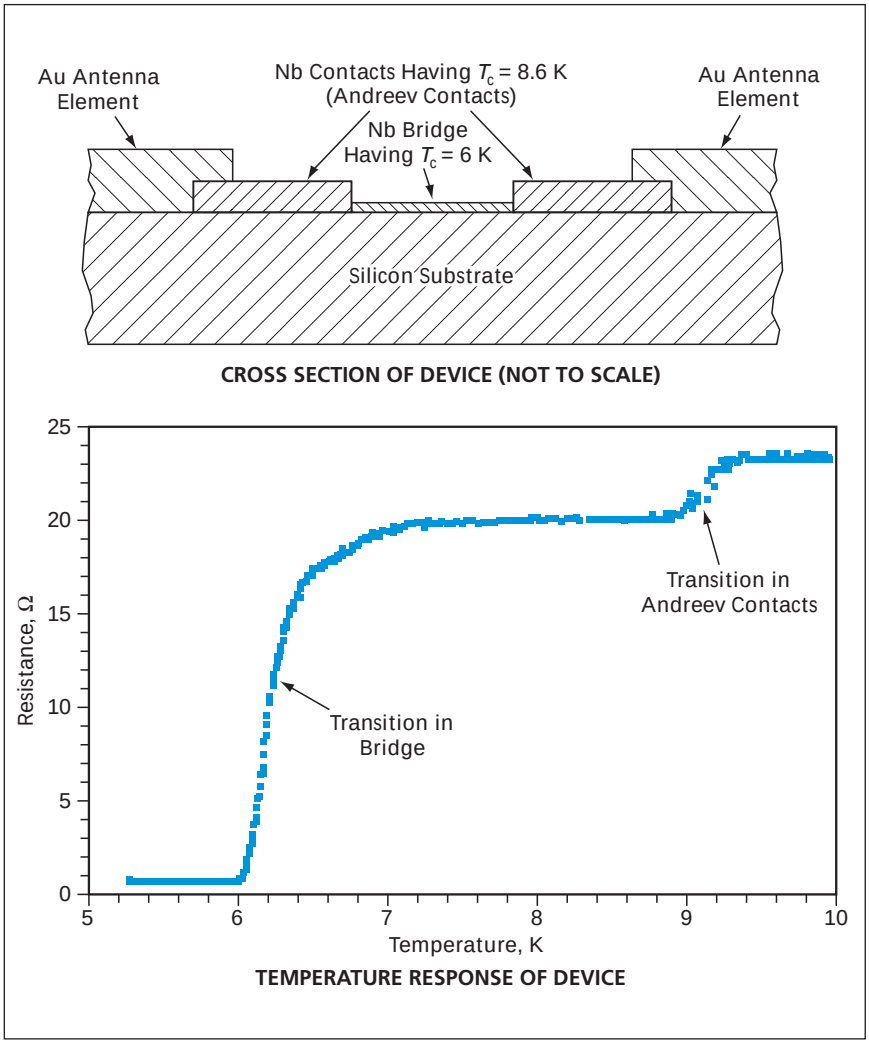

A **Thin Nb Bridge** having T_c = 6 K lies between thicker Nb contacts having T_c = 8.6 K that, in turn, are connected to an antenna that couples submillimeter-wavelength radiation into the device.

the approach followed in developing the present device.

In the present device, the superconducting bridge having the T_c of 6 K is a thin film of niobium on a silicon substrate (see figure). This film is ≈1 μm wide, ≈1 μm long, and between 10 and 25 nm thick. A detector so small could lose some sensitivity if thermal energy were allowed to diffuse rapidly from the bridge into the contacts at the ends of the bridge. To minimize such diffusion, the contacts at the ends of the bridge are made from a 150-nm-thick niobium film that has a higher T_c(8.6 K). The interfaces between the bridge and the contacts constitute an energy barrier of sorts where Andreev reflection occurs. As a result, the sensitivity of the device depends primarily on thermal coupling between electrons and the crystal lattice in the Nb bridge. For this device, (NEP) = 2×10^{-14} W/Hz$^{1/2}$ and the response time is about 0.5 ns.

In order to obtain high quantum efficiency, a planar spiral gold antenna is connected to the niobium contacts. The antenna enables detection of radiation throughout the frequency range from about 100 GHz to several terahertz. In operation, radiation is incident from the underside of the silicon substrate, and an antireflection-coated silicon lens (not shown in the figure) glued to the underside of the substrate focuses the radiation on the bridge (this arrangement is appropriate because silicon is transparent at submillimeter wavelengths).

*This work was done by Boris Karasik, William McGrath, and Henry Leduc of Caltech for NASA's Jet Propulsion Laboratory. Further information is contained in a TSP (see page 1).*NPO-43619

Large-Aperture Membrane Active Phased-Array Antennas

Large arrays are constructed as mosaics of smaller ones.

NASA's Jet Propulsion Laboratory, Pasadena, California

Large-aperture phased-array microwave antennas supported by membranes are being developed for use in spaceborne interferometric synthetic-aperture radar systems. There may also be terrestrial uses for such antennas supported on stationary membranes, large balloons, and blimps. These antennas are expected to have areal mass densities of about 2 kg/m^2, satisfying a need for lightweight alternatives to conventional rigid phased-array antennas, which have typical areal mass densities between 8 and 15 kg/m^2. The differences in areal mass densities translate to substantial differences in total mass in contemplated applications involving aperture areas as large as 400 m^2.

A membrane phased-array antenna includes patch antenna elements in a repeating pattern. All previously reported membrane antennas were passive antennas; this is the first active membrane antenna that includes transmitting/receiving (T/R) electronic circuits as integral parts. Other integral parts of the antenna include a network of radio-frequency (RF) feed lines (more specifically, a corporate feed network) and of bias and control lines, all in the form of flexible copper strip conductors on flexible polymeric membranes.

Each unit cell of a prototype antenna (see Figure 1) contains a patch antenna element and a compact T/R module that is compatible with flexible membrane circuitry. There are two membrane layers separated by a 12.7-mm air gap. Each membrane layer is made from a commercially available flexible circuit material that, as supplied, comprises a 127-μm-thick polyimide dielectric layer clad on both sides with 17.5-μm-thick copper layers. The copper layers are patterned into RF, bias, and control conductors. The T/R module is located on the back side of the ground plane

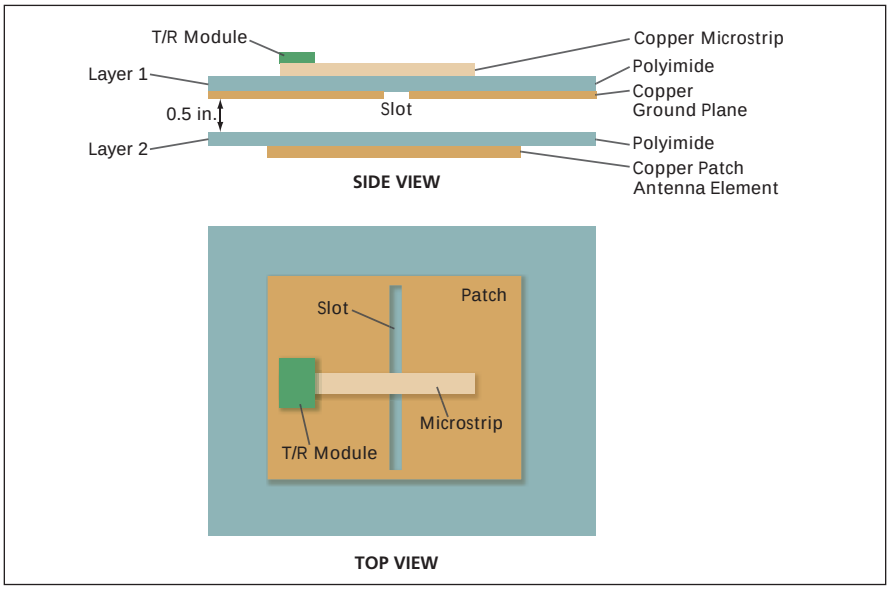

Figure 1. A **Unit Cell** of a phased-array antenna contains active and passive circuitry supported on two polyimide membrane layers.

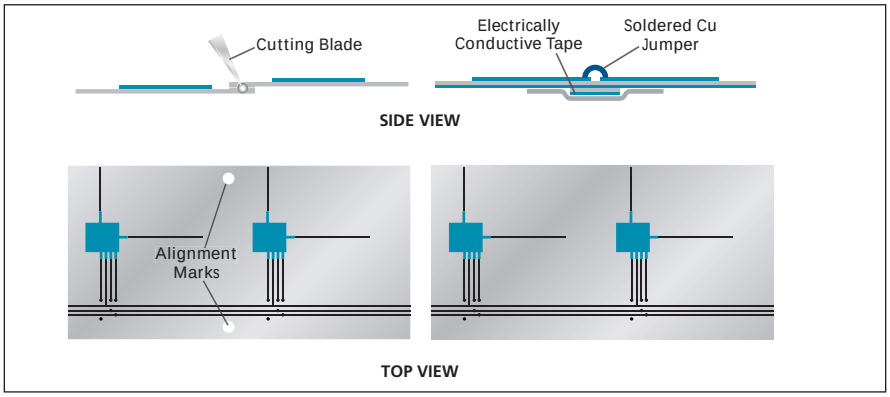

Figure 2. **Aligned Adjacent Panels** containing small (in this case, 1×2) membrane phased arrays are cut, then seamed together at the common cut line.

and is RF-coupled to the patch element via a slot. The T/R module is a hybrid multilayer module assembled and packaged independently and attached to the membrane array. At the time of reporting the information for this article, an 8×16 passive array (not including T/R modules) and a 2×4 active array (including T/R modules) had been demonstrated, and it was planned to fabricate and test larger arrays.

Because of limitations of available materials and equipment, the largest array that can be constructed as a single unit of the prototype design is a 2×8 array, which has dimensions of 0.28 m by 1.14 m. To construct a larger array, it is necessary to seam together 2×8 or smaller arrays. Figure 2 depicts selected aspects of the seaming process. Adjacent panels containing arrays to be seamed together are aligned using alignment marks on the panels and temporary tape. After the entire array has been aligned with temporary tape, the seams are match cut using an electric cutter. Finally, the cut panels are aligned, mechanically joined using a permanent adhesive and electrically joined using a combination of electrically conductive tape and soldered copper foil jumpers for the aforementioned conductive traces.

This work was done by Alina Moussessian, Mark Zawadzki, Ubaldo Quijano, Linda Del Castillo, and Etai Weininger of Caltech for NASA's Jet Propulsion Laboratory.

For more information, contact iaoffice@jpl.nasa.gov. NPO-45152

Optical Injection Locking of a VCSEL in an OEO

Compact, low-power atomic clocks could be developed.

NASA's Jet Propulsion Laboratory, Pasadena, California

Optical injection locking has been demonstrated to be effective as a means of stabilizing the wavelength of light emitted by a vertical-cavity surface-emitting laser (VCSEL) that is an active element in the frequency-control loop of an opto-electronic oscillator (OEO) designed to implement an atomic clock based on an electromagnetically-induced-transparency resonance. This particular optical-injection-locking scheme is expected to enable the development of small, low-power, high-stability atomic clocks that would be suitable for use in applications involving precise navigation and/or communication.

In one essential aspect of operation of an OEO of the type described above, a microwave modulation signal is coupled into the VCSEL. Heretofore, it has been well known that the wavelength of light emitted by a VCSEL depends on its temperature and drive current, necessitating thorough stabilization of these operational parameters. Recently, it was discovered that the wavelength also depends on the microwave power coupled into the VCSEL. Inasmuch as the microwave power circulating in the frequency-control loop is a dynamic frequency-control variable (and, hence, cannot be stabilized), there arises a need for another means of stabilizing the wavelength.

The present optical-injection-locking scheme satisfies the need for a means to stabilize the wavelength against microwave-power fluctuations. It is also expected to afford stabilization against temperature and current fluctuations. In an experiment performed to demonstrate this scheme, wavelength locking was observed when about 200 μW of the output power of a commercial tunable diode laser was injected into a commercial

VCSEL, designed to operate in the wavelength range of 795±3 nm, that was generating about 200 μW of optical power. (The use of relatively high injection power levels is a usual practice in injection locking of VCSELs.)

This work was done by Dmitry Strekalov, Andrey Matsko, Anatoliy Savchenkov, Nan Yu, and Lute Maleki of Caltech for NASA's Jet Propulsion Laboratory. Further information is contained in a TSP (see page 1).

NPO-43454

Measuring Multiple Resistances Using Single-Point Excitation

Lyndon B. Johnson Space Center, Houston, Texas

In a proposed method of determining the resistances of individual DC electrical devices (e.g., batteries or fuel-cell stacks containing multiple electrochemical cells) connected in a series or parallel string, no attempt would be made to perform direct measurements on individual devices. Instead, (1) the devices would be instrumented by connecting reactive circuit components in parallel and/or in series with the devices, as appropriate; (2) a pulse or AC voltage excitation would be applied at a single point on the string; and (3) the transient or AC steady-state current response of the string would be measured at that point only. Each reactive component(s) associated with each device would be distinct in order to associate a unique time-dependent response with that device.

Using the known time-varying voltage excitation, the known values of inductance and/or capacitance, and the standard equation predicting the response for the known circuit configuration, the time-varying current response would be subjected to nonlinear regression analysis. In essence, this analysis would yield individual device resistances that result in a best fit between the predicted and actual time-varying current responses.

This work was done by Dan Hall of Lockheed Martin Corp. and Frank Davies of Hernandez Engineering, Inc. for Johnson Space Center. Further information is contained in a TSP (see page 1).

This invention is owned by NASA, and a patent application has been filed. Inquiries concerning nonexclusive or exclusive license for its commercial development should be addressed to the Patent Counsel, Johnson Space Center, (281) 483-1003. Refer to MSC-23623-1.

Improved-Bandwidth Transimpedance Amplifier

NASA's Jet Propulsion Laboratory, Pasadena, California

The widest available operational amplifier, with the best voltage and current noise characteristics, is considered for transimpedance amplifier (TIA) applications where wide bandwidth is required to handle fast rising input signals (as for time-of-flight measurement cases). The added amplifier inside the TIA feedback loop can be configured to have slightly lower voltage gain than the bandwidth reduction factor (the ratio of the input capacitance plus the feedback capacitance to the feed capacitance). This innovation enables the optimization of design based on suitable space-approved operational amplifiers and provides better, stronger performance under radiation and wide temperature variations. In many cases, this approach can eliminate the need to qualify new amplifiers.

This work was done by Jacob Chapsky of Caltech for NASA's Jet Propulsion Laboratory. For more information, contact iaoffice@jpl.nasa.gov.

NPO-45798

Inter-Symbol Guard Time for Synchronizing Optical PPM

This method would involve less computation than does the pilot-symbol method.

NASA's Jet Propulsion Laboratory, Pasadena, California

An inter-symbol guard time has been proposed as a means of synchronizing the symbol and slot clocks of an optical pulse-position modulation (PPM) receiver with the symbol and slot periods of an incoming optical PPM signal. (Such synchronization is necessary for correct identification of received symbols.) The proposal is applicable to the low-flux case in which the receiver photodetector operates in a photon-counting mode and the count can include contributions from incidental light sources and dark current. The use of the inter-symbol guard time would be an alternative to a prior synchronization method based on the periodic transmission of a fixed pilot symbol.

The proposal involves a modification of conventional M-ary optical PPM, in which each successive symbol period is divided into M time slots (0, 1, 2, ..., M-1), each slot being of duration T_s. Each time slot represents a different symbol in an alphabet of up to M symbols. At the transmitter, during each time slot, a laser either transmits a pulse or no pulse, depending on which symbol is to be sent. Synchronization of the receiver symbol and slot clocks is necessary because the task of the receiver is to determine which of the M possible symbols has been received by observing the photon counts accumulated during each of the M time slots of a symbol period.

In both the prior method and the method now proposed, the basic idea is to estimate the symbol and slot timing boundaries of the received signal by correlating the received-signal counts with a known component of the transmitted signal while taking account of the fact that the received-signal counts are related to the received-signal intensity through a Poisson distribution. In the prior method, the known component of

the transmitted signal is the pilot symbol, transmitted in place of an information symbol at intervals of R symbol periods. The pilot symbol is embodied as a pulse in the $M/2$th time slot of each affected Rth symbol period. In order to acquire the symbol and slot timing of the pilot signal, the receiver can correlate the received signal with variously delayed replicas of the pilot signal and choose the delay offset that yields the maximum correlation. The number of different correlations at increments of T_s is limited to MR; a coarse offset can thus be identified as whichever of these offsets yields the greatest correlation. Once the coarse offset has been determined, a finer estimate can be made by use of an early-late method with the adjacent correlation statistics.

In the method now proposed, there would be no pilot symbol. Instead, successive symbol periods would be separated by the aforementioned inter-symbol guard time, equal to one time slot T_s, during which no pulse would be transmitted. In effect, each symbol period would be divided into $M + 1$ time slots, of which the first M would be reserved for data pulses and the $M + 1$st, containing no pulse, would be used for synchronization. In this method, to acquire the symbol and slot timing of the received signal, one could seek either (1) the maximum correlation between the received signal and a synthetic signal consisting of pulses in all the data time slots or (2) the minimum correlation between the received signal and a synthetic signal consisting only of the inter-symbol guard time. In either case, the number of different correlations at increments of T_s would be limited to $M + 1$. As in the prior method, once the coarse offset had been determined, a finer estimate could be made by use of an early-late method with the adjacent correlation statistics.

Because fewer correlations would be needed to determine the coarse timing in the proposed method than are needed in the prior method, the proposed method could be implemented in a receiver by means of simpler, lower-power, less-massive computational circuitry, which is considered an acceptable trade-off to the slightly increased estimation error. Another advantage would be that unlike in the prior method, no energy would be expended in transmitting pilot symbols.

This work was done by William Farr, Jonathan Gin, and Meera Srinivasan of Caltech and Kevin Quirk of Northrop Grumman Information Technology for NASA's Jet Propulsion Laboratory. For further information, cintact iaoffice@jpl.nasa.gov.
NPO-43671

Novel Materials Containing Single-Wall Carbon Nanotubes Wrapped in Polymer Molecules

Coating carbon nanotubes in polymer molecules creates a new class of materials with enhanced mechanical properties for printed circuit boards, antenna arrays, and optoelectronics.

Lyndon B. Johnson Space Center, Houston, Texas

In this design, single-wall carbon nanotubes (SWNTs) have been coated in polymer molecules to create a new type of material that has low electrical conductivity, but still contains individual nanotubes, and small ropes of individual nanotubes, which are themselves good electrical conductors and serve as small conducting rods immersed in an electrically insulating matrix. The polymer is attached through weak chemical forces that are primarily non-covalent in nature, caused primarily through polarization rather than the sharing of valence electrons. Therefore, the electronic structure of the SWNT involved is substantially the same as that of free, individual (and small ropes of) SWNT. Their high conductivity makes the individual nanotubes extremely electrically polarizable, and materials containing these individual, highly polarizable molecules exhibit novel electrical properties including a high dielectric constant.

The polymer coating, however, greatly inhibits the Van der Waals attraction normally observed between separate, or small ropes of, SWNT. The polymer coating also interacts with solvents. The combination of the Van der Waals inhibition and the polymer-solvent interaction causes the wrapped nanotubes to be more readily suspended in solvents at high concentrations, which in turn substantially enables the manipulation of SWNT into many kinds of bulk materials including films, fibers, solids, and other types of composites. Also, the polymer-coated SWNT can be treated for the removal of the polymer molecules, restoring the SWNT to a pristine state.

Aggregations of the polymer-coated SWNT are substantially aligned and provide a new form of electrically-conducting rod composite, where the conducting rods have cross sectional dimensions on the nanometer scale and lengths of hundreds of nanometers or more. The electrical properties of the composite are highly anisotropic.

This innovation can be made compatible with matrices of other materials to facilitate fabrication of composites. Composite materials with polymer-coated SWNTs suspended in a polymer matrix have a novel structure of a suspended nanotube being smaller in its cross-sectional dimensions than the typical scale length of the individual polymer molecules in the matrix. This microscopic, dimensional compatibility minimizes the propensity of the composite to fail mechanically at the interface between the matrix and the SWNT, producing a composite material with enhanced properties such as strain-to-failure, toughness, and resistance to mechanical fatigue. These materials also serve as the active element for a range of transducers because they can change their physical dimensions in response to applied electric and magnetic fields. If treated with certain chemicals, the material can also change dimensionally and electronically in response to adsorption of chemicals on the nanotube surface, and can serve as chemical sensors and transducers.

This work was done by Richard E. Smalley and Michael J. O'Connell of Rice University and Kenneth Smith and Daniel T. Colbert of Carbon Nanotechnologies, Inc. for Johnson Space Center. For further information, contact the JSC Innovation Partnerships Office at (281) 483-3809.

In accordance with Public Law 96-517, the contractor has elected to retain title to this invention. Inquiries concerning rights for its commercial use should be addressed to:

William M. Rice University
Office of Technology Transfer
6100 Main Street
Houston, TX 77005
Phone No.: (713) 348-6188

Refer to MSC-24070-1, volume and number of this NASA Tech Briefs *issue, and the page number.*

Light-Curing Adhesive Repair Tapes

Adhesive resins in tapes are rigidized in place by exposure to light.

Marshall Space Flight Center, Alabama

Adhesive tapes, the adhesive resins of which can be cured (and thereby rigidized) by exposure to ultraviolet and/or visible light, are being developed as repair patch materials. The tapes, including their resin components, consist entirely of solid, low-outgassing, nonhazardous or minimally hazardous materials. They can be used in air or in vacuum and can be cured rapidly, even at temperatures as low as –20 °C. Although these tapes were originally intended for use in repairing structures in outer space, they can also be used on Earth for quickly repairing a wide variety of structures. They can be expected to be especially useful in situations in which it is necessary to rigidize tapes after wrapping them around or pressing them onto the parts to be repaired.

As now envisioned, when fully developed, the tapes would be tailored to specific applications and would be pack-

aged in light- and radiation-resistant, easy-to-use dispensers. The resins in the tapes would be formulated to be curable by low-power light at specific wavelengths that could be generated by light-emitting diodes (LEDs). Each such tape dispenser would be marketed as part of a repair kit that would also include a companion battery-powered LED source operating at the required wavelength.

Each tape consists of a fine-weave fabric impregnated by a resin. On one side of the tape there is a cover ply that prevents the tape from sticking to itself when it is rolled up as in a dispenser. Depending on the specific intended application, the cover ply and resin can be selected such that the cover ply can be either released from the tape or cured in place as an integral part of a repair patch.

The feasibility of the light-curing tapes was demonstrated in experiments in which tapes were made from fiberglass fabric impregnated, variously, with (1) cationic epoxy resins plus a sensitizer that preferentially absorbs light at a wavelength of 380 nm, (2) free-radical curing acrylate resins, or (3) blends of resins of both types. Methods of incorporating adducts into the epoxies to tailor their viscosities were developed. The tapes were applied to aluminum and carbon/epoxy composite substrates that had been prepared by sanding and wiping with alcohol. The resins were cured by 380-nm light from LEDs. The blends of resins of both types were found to be advantageous in that during exposure to the light, their acrylate components contributed rapid buildup of strength, while their epoxy components contributed adhesion and longer-term strength.

Poly(ethylene terephthalate) backing films were shown to pass the needed 380-nm light and, when prepared with corona treatment, to adhere well as parts of cured tapes. Peel tests confirmed generally high degrees of adhesion to aluminum substrates. Demonstrations of repairs were made, including bonding pipes of various materials together, patching burst pipes, and patching punctures. A 1-in. (2.54-cm) patch over a 1/2-in. (1.27-cm)-diameter hole was pressurized to 120 psi (≈0.83 MPa) without failure or delamination.

This work was done by Ronald Allred and Andrea Hoyt Haight of Adherent Technologies, Inc. for Marshall Space Flight Center. For further information, contact Sammy Nabors, MSFC Commercialization Assistance Lead, at sammy.a.nabors@nasa.gov. Refer to MFS-32532-1.

Thin-Film Solid Oxide Fuel Cells

Mass, volume, and the cost of materials can be reduced for a given power level.

Marshall Space Flight Center, Alabama

The development of thin-film solid oxide fuel cells (TFSOFCs) and a method of fabricating them have progressed to the prototype stage. A TFSOFC consists of the following:

- A fuel electrode (anode) of nickel or other suitable metal, about 10 micrometers thick, made porous in a required pattern as described below;
- A solid electrolyte deposited on the anode of 0.5- to 2-micrometer thickness;
- An oxidizer electrode (cathode) in the form of a layer of a mixed ionic-electronic conductive oxide deposited to a typical thickness between 1 and 10 micrometers on the solid-electrolyte face opposite that of the anode; and
- An electrically insulating structure that encloses the aforementioned components and includes manifolds for the delivery of fuel to the anode, delivery of air or other oxidizing gas mixture to the cathode, and removal of combustion products.

The porosity of the anode in a TFSOFC is necessary to enable delivery of the fuel to the anode side of the solid electrolyte. The cathode is required to be porous or at least permeable to the oxidizer to enable delivery of oxygen to the cathode side of the solid electrolyte. The solid electrolyte layer is required to be dense and free of defects so that neither the fuel nor the oxidizer leaks through it. The relatively small thickness of the electrolyte also makes it possible to operate the TFSOFC at temperature lower than is necessary for a thicker-electrolyte fuel cell of older design. In turn, operation at lower temperature increases the reliability and enables a wider choice of materials for constructing the TFSOFC.

In the fabrication of a TFSOFC, nickel foil to be used as the anode material can be rolled or otherwise processed to produce an ordered crystal structure so that subsequent epitaxial deposition of the solid electrolyte material on the anode will cause the solid electrolyte to be also crystallographically ordered and, therefore, to be dense and relatively free of defects, as required. The epitaxial deposition of the solid electrolyte and the deposition of the electronically and ionically conductive cathode layer on the electrolyte can be effected by any of several established processes for deposition of thin oxide films. After deposition of the solid electrolyte, the required porosity is introduced into the nickel by photolithographic patterning and etching.

The cathode layer can be deposited either before or after patterning of the anode. Optionally, to enhance the activity of the porous anode structure, a mixed-ionic-and-electronic-conductor film can be deposited on the anode patterning and etching.

Typically, the total thickness of the anode/solid electrolyte/cathode sandwich of a TFSOFC is only about 15–25 micrometers. Operating at a temperature between 450 and 500 °C, a TFSOFC can utilize hydrogen or methane as a fuel. The power density of a TFSOFC can exceed 10 W/cm^3 (10 kW/liter), while the power per unit mass is ≈3 W/g (or ≈3 kW/kg). Relative to older thicker-electrolyte fuel-cell designs, TFSOFC designs can reduce costs of materials and reduce the volumes and masses of fuel cells capable of a generating a given amount of electric power.

This work was done by Xin Chen, Nai-Juan Wu, and Alex Ignatiev of the University of Houston for Marshall Space Flight Center.

For further information, contact Sammy Nabors, MSFC Commercialization Assistance Lead, at sammy.a.nabors@nasa.gov. Refer to MFS-32513-1

Zinc Alloys for the Fabrication of Semiconductor Devices

Materials improve the performance of semiconductor devices.

Goddard Space Flight Center, Greenbelt, Maryland

ZnBeO and ZnCdSeO alloys have been disclosed as materials for the improvement in performance, function, and capability of semiconductor devices. The alloys can be used alone or in combination to form active photonic layers that can emit over a range of wavelength values.

Materials with both larger and smaller band gaps would allow for the fabrication of semiconductor heterostructures that have increased function in the ultraviolet (UV) region of the spectrum. ZnO is a wide band-gap material possessing good radiation-resistance properties. It is desirable to modify the energy band gap of ZnO to smaller values than that for ZnO and to larger values than that for ZnO for use in semiconductor devices. A material with band gap energy larger than that of ZnO would allow for the emission at shorter wavelengths for LED (light emitting diode) and LD (laser diode) devices, while a material with band gap energy smaller than that of ZnO would allow for emission at longer wavelengths for LED and LD devices.

The amount of Be in the ZnBeO alloy system can be varied to increase the energy bandgap of ZnO to values larger than that of ZnO. The amount of Cd and Se in the ZnCdSeO alloy system can be varied to decrease the energy band gap of ZnO to values smaller than that of ZnO. Each alloy formed can be undoped or can be p-type doped using selected dopant elements, or can be n-type doped using selected dopant elements.

The layers and structures formed with both the ZnBeO and ZnCdSeO semiconductor alloys — including undoped, p-type-doped, and n-type-doped types — can be used for fabricating photonic and electronic semiconductor devices for use in photonic and electronic applications. These devices can be used in LEDs, LDs, FETs (field effect trasnstors), PN junctions, PIN junctions, Schottky barrier diodes, UV detectors and transmitters, and transistors and transparent transistors. They also can be used in applications for light-emitting display, backlighting for displays, UV and visible transmitters and detectors, high-frequency radar, biomedical imaging, chemical compound identification, molecular identification and structure, gas sensors, imaging systems, and for the fundamental studies of atoms, molecules, gases, vapors, and solids.

This work was done by Yungryel Ryu, Tae S. Lee, and Henry W. White of MOXtronics for Goddard Space Flight Center. Further information is contained in a TSP (see page 1). ***GSC-15634-1***

Small, Lightweight, Collapsible Glove Box

The box is easily prepared for performing experiments in limited work space.

Ames Research Center, Moffett Field, California

A small, lightweight, collapsible glove box enables its user to perform small experiments and other tasks. Originally intended for use aboard a space shuttle or the International Space Station (ISS), this glove box could also be attractive for use on Earth in settings in which work space or storage space is severely limited and, possibly, in which it is desirable to minimize weight.

The development of this glove box was prompted by the findings that in the original space-shuttle or ISS setting, (1) it was necessary to perform small experiments in a large general-purpose work station, so that, in effect, they occupied excessive space; and it took excessive amounts of time to set up small experiments. The design of the glove box reflects the need to minimize the space occupied by experiments and the time needed to set up experiments, plus the requirement to limit the launch weight of the box and the space needed to store the box during transport into orbit.

To prepare the glove box for use, the astronaut or other user has merely to insert hands through the two fabric glove ports in the side walls of the box and move two hinges to a locking vertical position (see figure). The user could do this while seated with the glove box on the user's lap. When stowed, the glove box is flat and has approximately the thickness of two pieces of 8-in. (≈20 cm) polycarbonate.

This work was done by Jerry James of Lockheed Martin for Ames Research Center. Further information is contained in a TSP (see page 1).

Inquiries concerning rights for the commercial use of this invention should be addressed to the Ames Technology Partnerships Division at (650) 604-2954. Refer to ARC-15179-1.

Only Simple Motions are needed to prepare the glove box for use.

Radial Halbach Magnetic Bearings

Complex active control systems are not necessary for stable levitation.

John H. Glenn Research Center, Cleveland, Ohio

Radial Halbach magnetic bearings have been investigated as part of an effort to develop increasingly reliable noncontact bearings for future high-speed rotary machines that may be used in such applications as aircraft, industrial, and land-vehicle power systems and in some medical and scientific instrumentation systems. Radial Halbach magnetic bearings are based on the same principle as that of axial Halbach magnetic bearings, differing in geometry as the names of these two types of bearings suggest. Both radial and axial Halbach magnetic bearings are passive in the sense that unlike most other magnetic bearings that have been developed in recent years, they effect stable magnetic levitation without need for complex active control.

Axial Halbach magnetic bearings were described in "Axial Halbach Magnetic Bearings" (LEW-18066-1), *NASA Tech Briefs*, Vol. 32, No. 7 (July 2008), page 85. In the remainder of this article, the description of the principle of operation from the cited prior article is recapitulated and updated to incorporate the present radial geometry.

In simplest terms, the basic principle of levitation in an axial or radial Halbach magnetic bearing is that of the repulsive electromagnetic force between (1) a moving permanent magnet and (2) an electric current induced in a stationary electrical conductor by the motion of the magnetic field. An axial or radial Halbach bearing includes multiple permanent magnets arranged in a Halbach array ("Halbach array" is defined below) in a rotor and multiple conductors in the form of wire coils in a stator, all arranged so the rotary motion produces an axial or radial repulsion that is sufficient to levitate the rotor.

A basic Halbach array (see Figure 1) consists of a row of permanent magnets, each oriented so that its magnetic field is

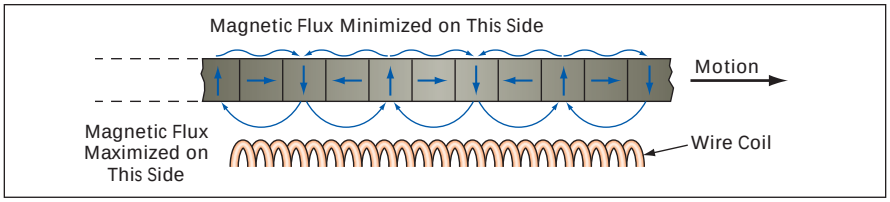

Figure 1. A **Basic Halbach Array** consists of permanent magnets oriented in a sequence of quarter turns chosen to concentrate the magnetic field on one side. The motion of the array along a wire coil gives rise to an electromagnetic repulsion that can be exploited for levitation.

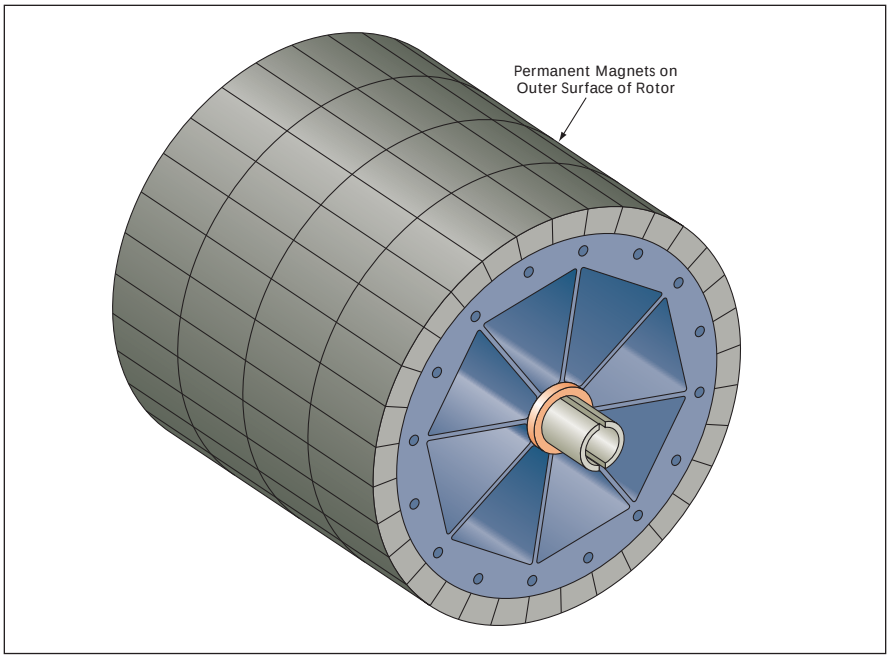

Figure 2. The **Rotor in a Radial Halbach Magnetic Bearing** has an outer layer consisting of a cylindrical version of the Halbach array of Figure 1. The bearing also includes multiple coils in a stator (omitted from this view) surrounding the rotor.

at a right angle to that of the adjacent magnet, and the right-angle turns are sequenced so as to maximize the magnitude of the magnetic flux density on one side of the row while minimizing it on the opposite side. The advantage of this configuration is that it makes it possible to approach the theoretical maximum force per unit area that could be exerted by a given amount of permanent-magnet material. The configuration is named after physicist Klaus Halbach, who conceived it for use in particle accelerators. Halbach arrays have also been studied for use in magnetic-levitation ("maglev") railroad trains.

In a radial Halbach magnetic bearing, the basic Halbach arrangement is modified into a symmetrical arrangement of sector-shaped permanent magnets mounted on the outer cylindrical surface of a drum rotor (see Figure 2). The magnets are oriented to concentrate the magnetic field on their radially outermost surface. The stator coils are mounted in a stator shell surrounding the rotor.

At a given radial position on the outer rotor magnet surface, the magnetic flux along any given direction varies approximately sinusoidally with the circumferential coordinate. When the disk rotates, the temporal variation of the magnetic field intercepted by the stator coils induces electric currents, thereby generating a repulsive electromagnetic force. The circuits of the stator coils are typically closed by inductors, the values of which are chosen to modify the phase shifts of voltage and currents so as to maximize the radial repulsion. Above a critical speed that depends on the specific design, the repulsive force is sufficient to levitate the rotor. During startup, shutdown, and other events in which the rate of rotation falls below the critical speed, the rotor comes to rest on an auxiliary mechanical bearing.

This work was done by Dennis J. Eichenberg, Christopher A. Gallo, and William K. Thompson of Glenn Research Center. Further information is contained in a TSP (see page 1).

Inquiries concerning rights for the commercial use of this invention should be addressed to NASA Glenn Research Center, Innovative Partnerships Office, Attn: Steve Fedor, Mail Stop 4–8, 21000 Brookpark Road, Cleveland, Ohio 44135. Refer to LEW-18239-1.

Aerial Deployment and Inflation System for Mars Helium Balloons

Various factors are considered to ensure mission success.

NASA's Jet Propulsion Laboratory, Pasadena, California

A method is examined for safely deploying and inflating helium balloons for missions at Mars. The key for making it possible to deploy balloons that are light enough to be buoyant in the thin, Martian atmosphere is to mitigate the transient forces on the balloon that might tear it.

A fully inflated Mars balloon has a diameter of 10 m, so it must be folded up for the trip to Mars, unfolded upon arrival, and then inflated with helium gas in the atmosphere. Safe entry into the Martian atmosphere requires the use of an aeroshell vehicle, which protects against severe heating and pressure loads associated with the hypersonic entry flight. Drag decelerates the aeroshell to supersonic speeds, then two parachutes deploy to slow the vehicle down to the needed safe speed of 25 to 35 m/s for balloon deployment. The parachute system descent dynamic pressure must be approximately 5 Pa or lower at an altitude of 4 km or more above the surface.

At this point, a pyrotechnic device will break the retaining mechanism and open the balloon container. The parachute force will pull the balloon upwards out of the container while simultaneously the payload module (containing the helium tanks and flow control sys-

tem) freefalls and pulls the bottom of the balloon down. This causes the balloon to stretch out to its maximum length. Transient shock loads are generated in the balloon when its maximum length is reached. These shock loads are held to safe values by ripstitch elements in the flight train that break at a prescribed force and dissipate energy. After a short delay, a valve opens to start the helium flow into the bottom of the balloon through a flexible hose connector. Pyrotechnic cutting devices fire at the end of inflation to stop the helium flow and to separate the parachute and payload module from the balloon. By design, the balloon ends inflation below its nominal float altitude to avoid over-pressurization. It will then rise to its nominal float altitude, typically 2 km or more above the surface, before leveling off. This may require some venting of excess helium through a pressure relief valve.

At the time of this reporting, this technology is at the prototype testing stage. Further development is needed, particularly with end-to-end flight tests showing the balloon surviving deployment and floating afterward, as well as increasing the size of the balloon from its current 10-m diameter to an ultimate size of 20 m in order to support equatorial Mars missions.

This work was done by Tim Lachenmeier of Near Space Corp.; Debora Fairbrother and Chris Shreves of NASA-Wallops; and Jeffery L. Hall, Viktor V. Kerzhanovich, Michael T. Pauken, Gerald J. Walsh, and Christopher V. White of Caltech for NASA's Jet Propulsion Laboratory. For more information, contact iaoffice@jpl.nasa.gov. NPO-44688

Steel Primer Chamber Assemblies for Dual Initiated Pyrovalves

NASA's Jet Propulsion Laboratory, Pasadena, California

A solution was developed to mitigate the potential risk of ignition failures and burn-through in aluminum primer chamber assemblies on pyrovalves. This was accomplished by changing the assembly material from aluminum to steel, and reconfiguration of flame channels to provide more direct paths from initiators to boosters. With the geometric configuration of the channels changed, energy is more efficiently transferred from the initiators to the boosters. With the alloy change to steel, the initiator flame channels do not erode upon firing, eliminating the possibility of burn-through. Flight qualification tests have been successfully passed.

This work was done by Carl S. Guernsey and Masashi Mizukami of Caltech, Zac Zenz of Conax Florida Corp., and Adam A. Pender of Lockheed Martin Corp. for NASA's Jet Propulsion Laboratory. For more information, contact iaoffice@jpl.nasa.gov. NPO-46302

Voice Coil Percussive Mechanism Concept for Hammer Drill

NASA's Jet Propulsion Laboratory, Pasadena, California

A hammer drill design of a voice coil linear actuator, spring, linear bearings, and a hammer head was proposed. The voice coil actuator moves the hammer head to produce impact to the end of the drill bit. The spring is used to store energy on the retraction and to capture the rebound energy after each impact for use in the next impact. The maximum actuator stroke is 20 mm with the hammer mass being 200 grams. This unit can create impact energy of 0.4 J with 0.8 J being the maximum.

This mechanism is less complex than previous devices meant for the same task, so it has less mass and less volume. Its impact rate and energy are easily tunable without changing major hardware components. The drill can be driven by two half-bridges. Heat is removed from the voice coil via CO_2 conduction.

This work was done Avi Okon of Caltech for NASA's Jet Propulsion Laboratory. For more information, contact iaoffice@jpl.nasa.gov. NPO-45712

Inherently Ducted Propfans and Bi-Props

Noise would be reduced without the weight and other disadvantages of shrouds.

Langley Research Center, Hampton, Virginia

The terms "inherently ducted propfan" (IDP) and "inherently ducted biprop" (IDBP) denote members of a proposed class of propfan engines that would be quieter and would weigh less than do other propfan engines that generate equal amounts of thrust. The designs of these engines would be based on novel combinations of previously established aerodynamic-design concepts, including those of counter-rotating propfans, swept-back and swept-forward fixed wings, and ducted propfans.

Heretofore, noise-reducing propfan designs have provided for installation of shrouds around the blades. A single propeller surrounded by such a shroud is denoted an advanced ducted propeller (ADP); a pair of counter-rotating propellers surrounded by such a shroud is denoted a counter-rotating integrated shrouded propeller (CRISP). In addition to adding weight, the shrouds engender additional undesired rotor/stator interactions and cascade effects, and contribute to susceptibility to choking.

An IDP or IDBP would offer some shielding against outward propagation of noise, similar to shielding by a shroud, but without the weight and other undesired effects associated with shrouds. An IDP would include a pair of counter-rotating propellers. The

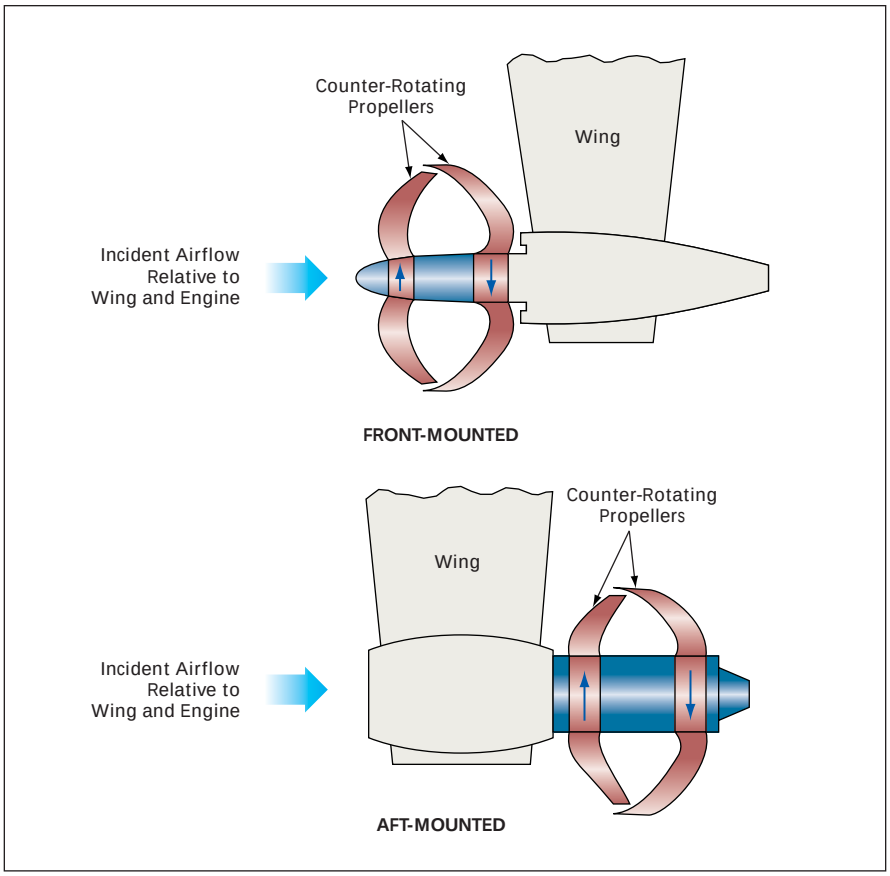

An **IDP Would Be a Counter-Rotating Propfan** with scimitar type blade design. The propellers could be located forward or aft, relative to the wing.

blades of the upstream propeller would be swept back, while those of the downstream propeller would be swept forward (see figure). The downstream blades would have a geometric twist such that their forward-swept tips could act as winglets extending over the tips of the upstream blades. In principle, the resulting periodic coverage of the upstream-blade tips by the downstream-blade tips would suppress outward propagation of noise, as though a short noise-shielding duct were present. Furthermore, it is anticipated that an IDP would be less susceptible to some of the operational limitations of a CRISP during asymmetric flow conditions or reverse thrust operation.

An IDBP would be based on the same principles as those of an IDP, except for one major difference: In an IDBP, to enhance structural integrity, pairs of the blades of the downstream propeller would be connected by the winglets. This arrangement is particularly suitable for high solidity installations and can reduce overall weight and drag as compared to a rotating shroud concept.

This work was done by M. A. Takallu of Langley Research Center. For further information, contact the Langley Innovative Partnerships Office at (757) 864-4015.
LAR-15031-1

Silicon Nanowire Growth at Chosen Positions and Orientations

There are numerous potential applications in highly miniaturized sensors and electronic devices.

Goddard Space Flight Center, Greenbelt, Maryland

It is now possible to grow silicon nanowires at chosen positions and orientations by a method that involves a combination of standard microfabrication processes. Because their positions and orientations can be chosen with unprecedented precision, the nanowires can be utilized as integral parts of individually electronically addressable devices in dense arrays.

Nanowires made from silicon and perhaps other semiconductors hold substantial promise for integration into highly miniaturized sensors, field-effect transistors, optoelectronic devices, and other electronic devices. Like bulk semiconductors, inorganic semiconducting nanowires are characterized by electronic energy bandgaps that render them suitable as means of modulating or controlling electronic signals through electrostatic gating, in response to incident light, or in response to molecules of interest close to their surfaces. There is now potential for fabricating arrays of uniform, individually electronically addressable nanowires tailored to specific applications.

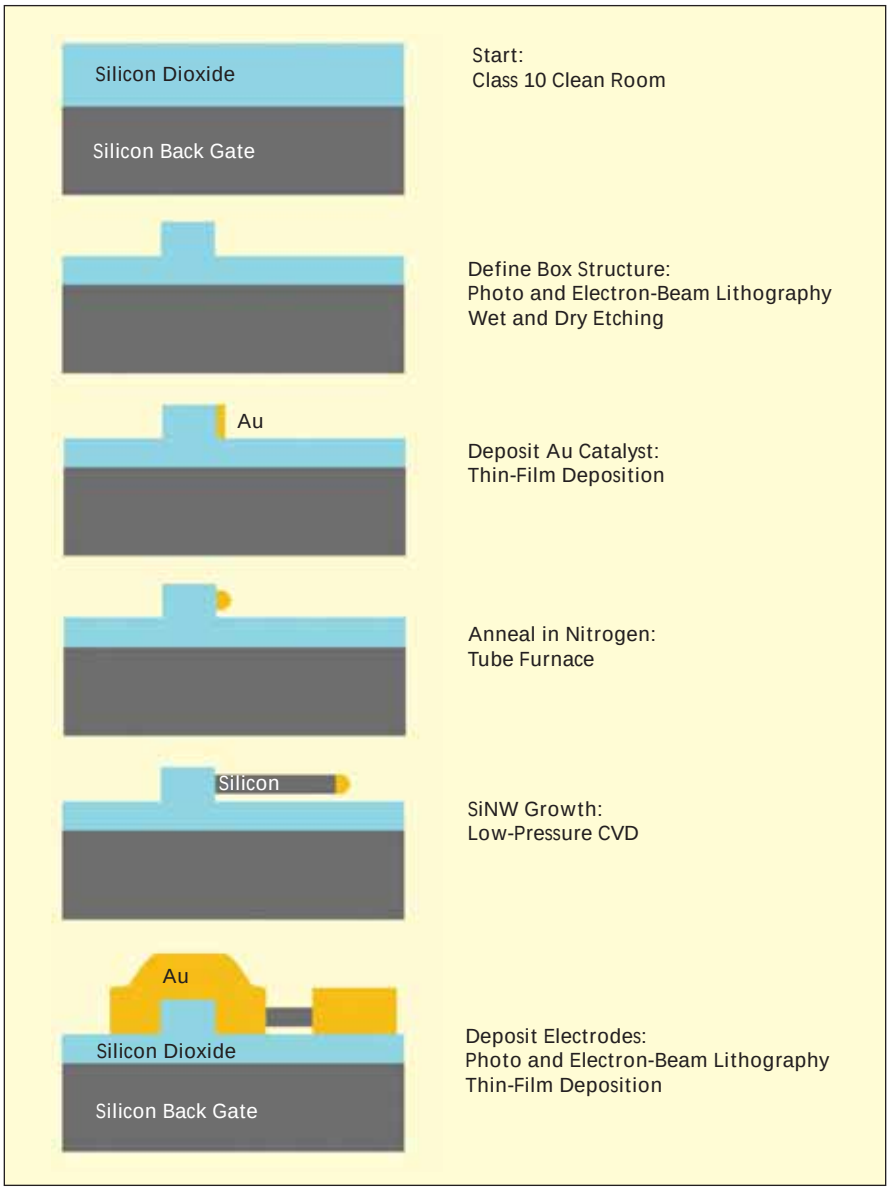

Gold Particles on substrate surfaces catalyze the growth of silicon nanowires by chemical vapor deposition. The nanowires grow outward, carrying the gold particles at their tips. The nanowires can be grown across gaps to form nanobridges.

The method involves formation of metal catalytic particles at the desired positions on a substrate, followed by heating the substrate in the presence of silane gas. The figure illustrates an example in which a substrate includes a silicon dioxide surface layer that has been etched into an array of pillars and the catalytic (in this case, gold) particles have been placed on the right-facing sides of the pillars. The catalytic thermal decomposition of the silane to silicon and hydrogen causes silicon columns (the desired nanowires) to grow outward from the originally catalyzed spots on the substrate, carrying the catalytic particles at their tips. Thus, the position and orientation of each silicon nanowire is determined by the position of its originally catalyzed spot on the substrate surface, and the orientation of the nanowire is perpendicular to the substrate surface at the originally catalyzed spot.

The diameter of the nanowire is determined by the diameter of its catalytic particle. In principle, using this technique, the diameter of the silicon nanowire can be controlled precisely by the dimensions of the surface pillar. In the example of the figure, the positions and diameter of the catalytic particles are determined as follows: The right-facing pillar surfaces are coated with gold in a directional evaporative deposition process. The deposition thickness is chosen in conjunction with the area of the pillar faces so that the amount of gold on each face is such that if the gold were aggregated into a hemisphere at the center of each face, the diameter of the hemisphere would equal the desired di-

ameter of the nanowires to be grown from the pillar faces. The aggregation is effected by heating the workpiece in an inert atmosphere.

The pillar array can then be used as a reference mark for straightforward device fabrication in a process called alignment. Knowing the position of the silicon nanowires avoids the present difficulties of working with random or semi-random distributions of silicon nanowires. In an important class of potential applications, nanobridges would be coated with biomolecules (e.g., antigens) that bind to other biomolecules of interest (e.g., the antibodies corresponding to the antigens) to enable highly sensitive detection of the molecules of interest. Sensors comprising arrays of multiplexed nanobridges functionalized for detection of proteins symptomatic of cancer have already been demonstrated to be feasible.

This work was done by Stephanie A Getty of Goddard Space Flight Center. Further information is contained in a TSP (see page 1).
GSC-15368-1

Detecting Airborne Mercury by Use of Gold Nanowires

Mercury has been detected at concentrations as low as 2 ppb.

NASA's Jet Propulsion Laboratory, Pasadena, California

Like the palladium chloride ($PdCl_2$) films described in the immediately preceding article, gold nanowire sensors have been found to be useful for detecting airborne elemental mercury at concentrations on the order of parts per billion (ppb). Also like the $PdCl_2$ films, gold nanowire sensors can be regenerated under conditions much milder than those necessary for regeneration of gold films that have been used as airborne-Hg sensors. The interest in nanowire sensors in general is prompted by the expectation that nanowires of a given material covering a given surface may exhibit greater sensitivity than does a film of the same material because nanowires have a greater surface area.

In preparation for experiments to demonstrate this sensor concept, sensors were fabricated by depositing gold nanowires, variously, on microhotplate or microarray sensor substrates. In the experiments, the electrical resistances were measured while the sensors were exposed to air at a temperature of 25 °C and relative humidity of about 30 percent containing mercury at various concentrations from 2 to 70 ppb (see figure). The results of this and other experiments have been interpreted as signifying that sensors of this type can detect mercury at ppb concentrations in room-temperature air and can be regenerated by exposure to clean flowing air at temperatures <40 °C.

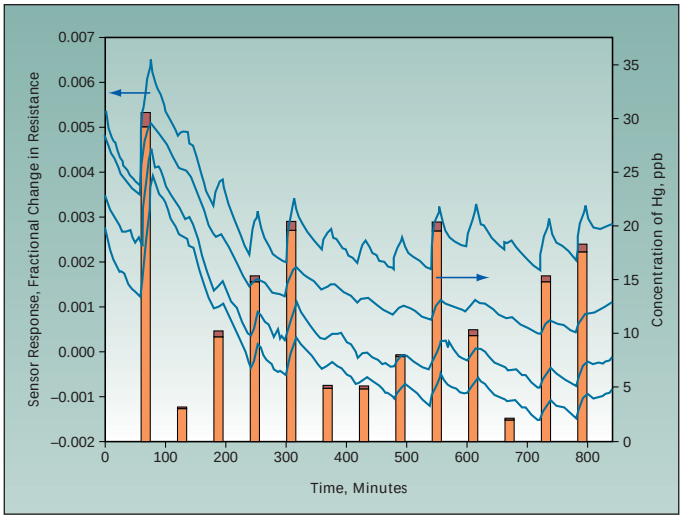

Four Gold-Nanowire-Mat Sensors were exposed to various concentrations of Hg in air at a temperature of 25 °C and a relative humidity of about 30 percent.

The responses of the experimental sensors were found to be repeatable over a period of about 4 months, to vary approximately linearly with concentration from 2 to 20 ppb, and to vary somewhat nonlinearly with concentration above 20 ppb. Although mercury concentrations were found to be measurable down to 2 ppb, the limit of sensitivity may be lower than 2 ppb: Experiments at lower concentrations had not yet been performed at the time of reporting the information for this article.

This work was done by Margaret Ryan, Abhijit Shevade, Adam Kisor, and Margie Homer of Caltech; Jessica Soler of Glendale City College; and Nosang Myung and Megan Nix of the University of California, Riverside, for NASA's Jet Propulsion Laboratory. Further information is contained in a TSP (see page 1). *NPO-44787*

Detecting Airborne Mercury by Use of Palladium Chloride

These sensors can be regenerated under relatively mild conditions.

NASA's Jet Propulsion Laboratory, Pasadena, California

Palladium chloride films have been found to be useful as alternatives to the gold films heretofore used to detect airborne elemental mercury at concentrations of the order of parts per billion (ppb). Somewhat more specifically, when suitably prepared palladium chloride films are exposed to parts-per-billion or larger concentrations of airborne mercury, their electrical resistances change by amounts large enough to be easily measurable. Because airborne mercury adversely affects health, it is desirable to be able to detect it with high sensitivity, especially in enclosed environments in which there is a risk of leakage of mercury from lamps or other equipment.

The detection of mercury by use of gold films involves the formation of gold/mercury amalgam. Gold films

offer adequate sensitivity for detection of airborne mercury and could easily be integrated into an electronic-nose system designed to operate in the temperature range of 23 to 28 °C. Unfortunately, in order to regenerate a gold-film mercury sensor, one must heat it to a temperature of 200 °C for several minutes in clean flowing air.

In preparation for an experiment to demonstrate the present sensor concept, palladium chloride was deposited from an aqueous solution onto sets of gold electrodes and sintered in air to form a film. Then while using the gold electrodes to measure the electrical resistance of the films, the films were exposed, at a temperature of 25 °C, to humidified air containing mercury at various concentrations from 0 to 35 ppb (see figure). The results of this and other experiments have been interpreted as signifying that sensors of this type can detect mercury in room-temperature air at concentrations of at least 2.5 ppb and can readily be regenerated at temperatures <40 °C.

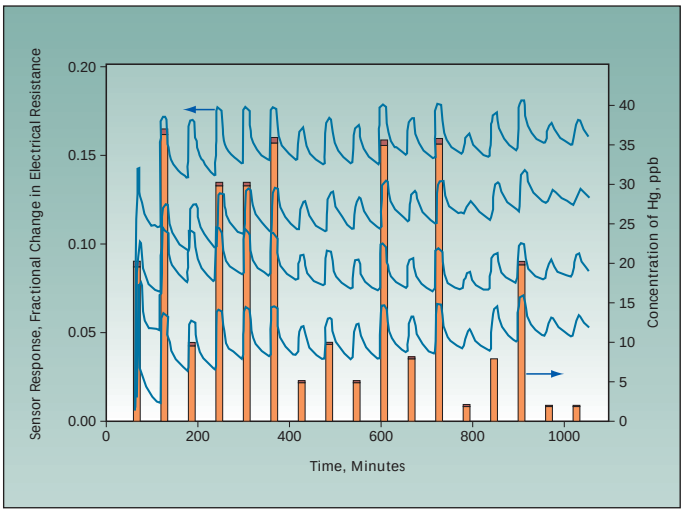

Four $PdCl_2$-Film Sensors were exposed to various concentrations of Hg in air at a temperature of 25 °C and a relative humidity of 31 percent.

This work was done by Margaret Ryan, Abhijit Shevade, Adam Kisor, Margie Homer, and April Jewell of Caltech; Kenneth Manatt of Santa Barbara Research; Julia Torres and Jessica Soler of Glendale College; and Charles Taylor of Pomona College for NASA's Jet Propulsion Laboratory. urther information is contained in a TSP (see page 1).

In accordance with Public Law 96-517, the contractor has elected to retain title to this invention. Inquiries concerning rights for its commercial use should be addressed to:

Innovative Technology Assets Management
JPL
Mail Stop 202-233
4800 Oak Grove Drive
Pasadena, CA 91109-8099
E-mail: iaoffice@jpl.nasa.gov

Refer to NPO-44955, volume and number of this NASA Tech Briefs *issue, and the page number.*

Micro Electron MicroProbe and Sample Analyzer

EDX and high-resolution microscopy could be performed in the field.

NASA's Jet Propulsion Laboratory, Pasadena, California

A proposed, low-power, backpack-sized instrument, denoted the micro electron microprobe and sample analyzer (MEMSA), would serve as a means of rapidly performing high-resolution microscopy and energy-dispersive x-ray spectroscopy (EDX) of soil, dust, and rock particles in the field. The MEMSA would be similar to an environmental scanning electron microscope (ESEM) but would be much smaller and designed specifically for field use in studying effects of geological alteration at the micrometer scale. Like an ESEM, the MEMSA could be used to examine uncoated, electrically nonconductive specimens. In addition to the difference in size, other significant differences between the MEMSA and an ESEM lie in the mode of scanning and the nature of the electron source.

The MEMSA (see figure) would include an electron source that would focus a beam of electrons onto a small spot on a specimen, which would be mounted on a three-axis translation stage in a partly evacuated sample-exchange chamber. Whereas the electron sources in other SEMs typically contain thermionic cathodes, the electron source in the MEMSA would contain a field-emission cathode containing a planar array of bundles of carbon nanotubes (CNTs). Cathodes of this type are capable of high current densities (tens of amperes per square centimeter) at very low fields (8 to 10 V/μm), and the arrays of bundles of CNTs in them are amenable to fabrication within designated areas of the order of a few square nanometers, making it possible to focus electron beams to small spots using simplified electron-beam optics. Another advantage of CNT field-emission cathodes is that they can tolerate operation in relatively poor vacuums [pressures of 10^{-5} to 10^{-4} torr (about 0.013 to 0.13 Pa)], which can be maintained by relatively small turbopumps, in contrast to the multistage pumps needed to maintain high vacuums required for thermionic cathodes.

As in an ESEM, the MEMSA would include a gaseous secondary-electron detector (GSED) for detecting secondary electrons excited by impingement of the electron beam on the specimen. Electrical charging of an electrically nonconductive specimen by the electron beam would be neutralized by impingement, on the specimen, of positive ions of the residual gas in the chamber. A Positive Intrinsic Negative (PIN) diode would be used as detector for energy-dispersive analysis of x rays generated in the impingement of the electron beam on the specimen.

Unlike in ESEMs and other SEMs, the electron beam would not be raster-scanned across the specimen. Instead, the electron beam would be focused on a fixed spot, through which the specimen would be moved in small steps by use of the translation stage to effect scanning. The amplified output of the GSED acquired at each step would be stored, along with the translation coordinates, in a digital memory, so that an image of the specimen could be reconstructed after completion of the scan. Omitted from the figure for the sake of simplicity is a context imager — essentially, a relatively-low-magnification electronic camera that would facilitate initial coarse positioning of the specimen in or near the electron-beam spot in preparation for scanning.

As in an ESEM, the sample-exchange chamber and the interior volume of the electron source would be separated by pressure-limiting apertures (PLAs), which are small apertures through which the electron beam passes on its way to the specimen. As in an ESEM, the PLAs would be sized to retard the flow of residual gas from the sample-exchange chamber to the electron source side so as to mainain the desired lower pressure

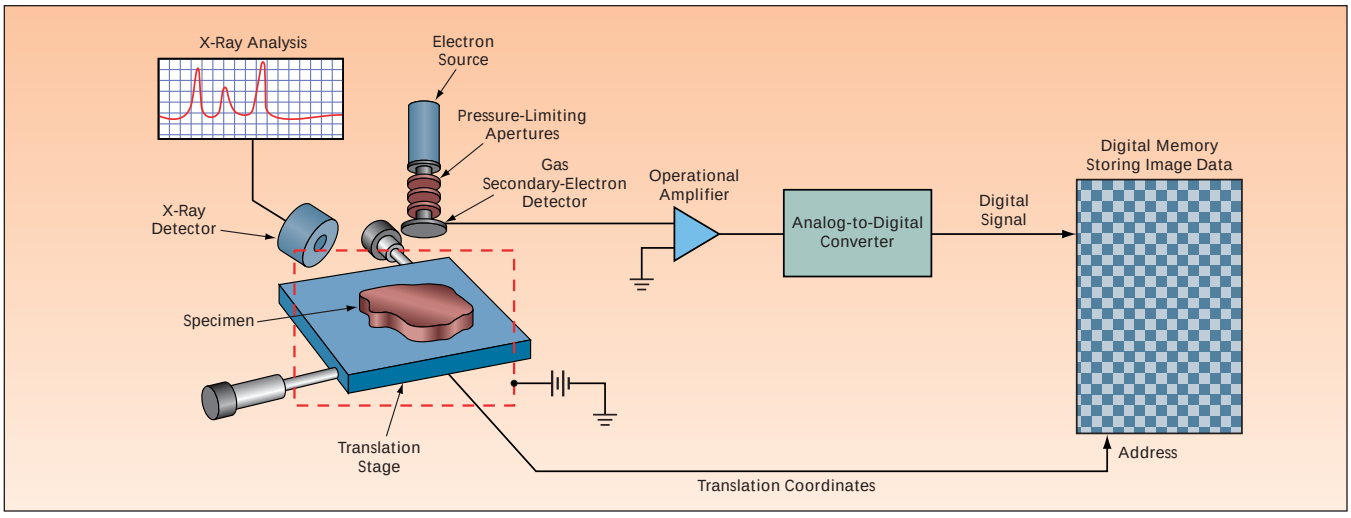

The **Micro Electron Probe and Sample Analyzer** would function similarly to an environmental scanning electron microscope but would differ in the nature of the electron source and the mode of scanning.

on the electron source side and the desired higher pressure in the sample-exchange chamber. In the original intended application of the MEMSA, the PLAs would be four platinum disks containing apertures of ≈0.5-mm diameter, chosen to maintain a pressure between 5 and 7 torr (about 0.67 to 0.93 kPa) of residual Martian atmospheric gas comprising primarily CO_2.

The MEMSA is expected to be capable of imaging at a spatial resolution of 40 nm or finer without EDX, or imaging at somewhat coarser resolution (of the order of 200 nm) with EDX in the energy range from 100 to 20 keV. The coarsening of resolution in the case of EDX would be a consequence of the need to use higher electron current. The maximum power demand of the MEMSA during operation has been estimated to be ≈5 W.

This work was done by Harish Manohara, Gregory Bearman, Susanne Douglas, Michael Bronikowski, Eduardo Urgiles, and Robert Kowalczyk, of Caltech and Charles Bryson of Apperati, Inc. for NASA's Jet Propulsion Laboratory.

In accordance with Public Law 96-517, the contractor has elected to retain title to this invention. Inquiries concerning rights for its commercial use should be addressed to:

Innovative Technology Assets Management
JPL
Mail Stop 202-233
4800 Oak Grove Drive
Pasadena, CA 91109-8099
E-mail: iaoffice@jpl.nasa.gov

Refer to NPO-45389, volume and number of this NASA Tech Briefs *issue, and the page number.*

Nanowire Electron Scattering Spectroscopy

Multiple chemical compounds could be sensed, without the need to chemically functionalize nanowires.

NASA's Jet Propulsion Laboratory, Pasadena, California

Nanowire electron scattering spectroscopy (NESS) has been proposed as the basis of a class of ultra-small, ultra-low-power sensors that could be used to detect and identify chemical compounds present in extremely small quantities. State-of-the-art nanowire chemical sensors have already been demonstrated to be capable of detecting a variety of compounds in femtomolar quantities. However, to date, chemically specific sensing of molecules using these sensors has required the use of chemically functionalized nanowires with receptors tailored to individual molecules of interest. While potentially effective, this functionalization requires labor-intensive treatment of many nanowires to sense a broad spectrum of molecules. In contrast, NESS would eliminate the need for chemical functionalization of nanowires and would enable the use of the same sensor to detect and identify multiple compounds.

NESS is analogous to Raman spectroscopy, the main difference being that in NESS, one would utilize inelastic scattering of electrons instead of photons to determine molecular vibrational energy levels. More specifically, in NESS, one would exploit inelastic scattering of electrons by low-lying vibrational quantum states of molecules attached to a nanowire or nanotube (see figure). The energy of the electrons is set by the voltage bias applied across the nanowire. When the electron energies correspond to particular molecular vibrational levels, enhanced electronic scattering will lead to a change in the differential conductance (dI/dV, where I is current and V is voltage) at that voltage. Thus changes in the conductance provide a direct readout of molecular vibrational energies, to enable spectroscopic identification of the attached molecules.

To realize a practical chemical sensor based on NESS, one would need a narrow-energy-band electron source, efficient coupling between the electrons and the molecules of interest, and the narrow vibrational bands in the molecules of interest. A carbon nanotube (CNT) provides a nearly ideal structure for satisfying the electron-source and coupling requirements for the following reasons: Even at room temperature, the energy bands in one dimensional carbon nanotubes are narrow, and low-energy electrons travel ballistically over distances of the order of a micron, so that injected electrons can have a nearly uniform kinetic energy. Because single-walled CNTs are essentially all "surface," there is strong coupling between electrons and molecules on their surfaces.

Other than CNTs, nanowires of silicon and perhaps other materials may yield usable NESS signals, though the signals are expected to be smaller than those from CNT-based sensors. One might need non-CNT nanowire NESS sensors to detect molecules that do not readily bind to CNTs.

In order to simplify the interpretation of a complex spectrum from a mixture of compounds, a NESS-based sensor could be integrated with a microfluidic

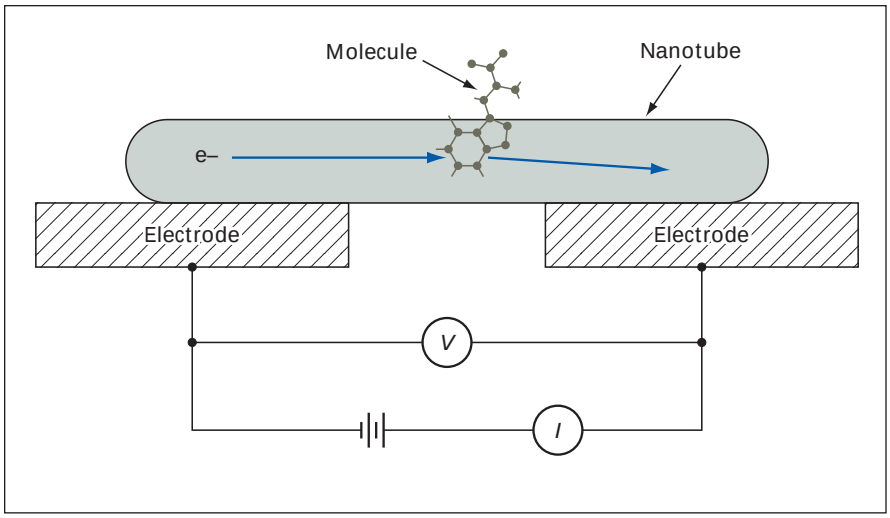

Inelastic Scattering of Electrons by molecules on the surface of a nanotube would affect the current-versus-voltage characteristic of the nanotube.

separation column. The column would enable separation and concentration of individual species, which would then be detected and identified at the column outlet by use of NESS.

This work was done by Brian Hunt, Michael Bronikowsky, Eric Wong, Paul Von Allmen, and Fabiano Oyafuso of Caltech for NASA's Jet Propulsion Laboratory. Further information is contained in a TSP (see page 1).

In accordance with Public Law 96-517, the contractor has elected to retain title to this invention. Inquiries concerning rights for its commercial use should be addressed to:

Innovative Technology Assets Management
JPL
Mail Stop 202-233
4800 Oak Grove Drive
Pasadena, CA 91109-8099
(818) 354-2240
E-mail: iaoffice@jpl.nasa.gov

Refer to NPO-42251, volume and number of this NASA Tech Briefs *issue, and the page number.*

Electron-Spin Filters Would Offer Spin Polarization >1

Net spin flux could be generated with little net electric current.

NASA's Jet Propulsion Laboratory, Pasadena, California

A proposal has been made to develop devices that would generate spin-polarized electron currents characterized by polarization ratios having magnitudes in excess of 1. Heretofore, such devices (denoted, variously, as spin injectors, spin polarizers, and spin filters) have typically offered polarization ratios having magnitudes in the approximate range of 0.01 to 0.1. The proposed devices could be useful as efficient sources of spin-polarized electron currents for research on spintronics and development of practical spintronic devices.

The polarization ratio in question — denoted the current spin polarization — is a standard measure of efficiency of a spin-polarizing device. It is defined in terms of current densities along a given coordinate axis, by means of the following equation:

$$P_J = (J\uparrow - J\downarrow) / (J\uparrow + J\downarrow),$$

where $J\uparrow$ is current density of electrons in the "up" spin state and $J\downarrow$ is the current density of electrons in the "down" spin state. If $J\uparrow$ and $J\downarrow$ can be made to have opposite signs — in other words, if electrons in opposite spin states can be made to move in opposite directions — then, as desired, it is possible to obtain $|P_J|>1$. By making $|P_J|>1$, one would make it possible to obtain a net spin flux with little net electric current.

A spin-polarizing device according to the proposal would be based largely on the same principles as those of the devices described in "Electron-Spin Filters Based on the Rashba Effect" (NPO-30635), *NASA Tech Briefs*, Vol. 28, No. 10 (October 2004), page 58. To recapitulate: The Rashba effect is an energy splitting, of what would otherwise be degenerate quantum states, caused by a spin-orbit interaction in conjunction with interfacial electric fields in an asymmetrical semiconductor heterostructure. The magnitude of the energy split is proportional to the electron wave number. Theoretically, electron-energy states would be split by the Rashba effect, and spin-polarized currents would be extracted by resonant quantum-mechanical tunneling. Accordingly, a spin-polarizing device based on these principles would be denoted an asymmetric resonant interband (or intraband, as the case may be) tunneling diode [a-RITD].

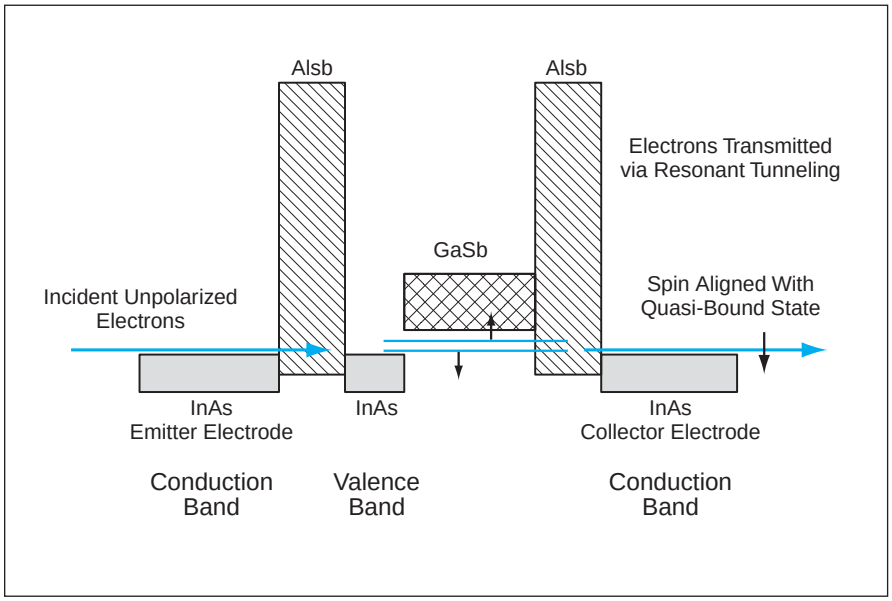

Electron-Energy-Band Alignments depicted here schematically are those of a proposed InAs/GaSb/AlSb a-RITD device for achieving current spin polarization >1. The shaded and cross-hatched regions represent bandgaps.

One possible structure of a device according to the present proposal would be similar to the a-RITD structure described previously: The device would comprise an asymmetric composite InAs-GaSb well, sandwiched between AlSb barriers and degenerately-n-doped InAs emitter and collector electrodes (see figure). Unpolarized electrons from the conduction band of the InAs emitter electrode would tunnel through one AlSb barrier and travel through an asymmetric InAs-GaSb quantum well, where Rashba spin splitting would occur; they would then tunnel through the other AlSb barrier into the conduction band of the InAs collector electrode. The device would be operated in an intraband-tunneling regime, in which no bias would be applied through the thickness of the stack of layers. A lateral electric (an electric field parallel to the planes of the layers) would be applied to emitter layer. With appropriately chosen thicknesses of layers and an appropriate value of the applied lateral electric field, it should be possible to achieve $|P_J|>1$.

This work was done by David Z. Ting of Caltech for NASA's Jet Propulsion Laboratory. Further information is contained in a TSP (see page 1).

NPO-30670

Subcritical-Water Extraction of Organics From Solid Matrices

An environmentally benign solvent is used in a simple extraction process.

NASA's Jet Propulsion Laboratory, Pasadena, California

An apparatus for extracting organic compounds from soils, sands, and other solid matrix materials utilizes water at subcritical temperature and pressure as a solvent. The apparatus, called subcritical water extractor (SCWE), is a prototype of subsystems of future instrumentation systems to be used in searching for organic compounds as signs of past or present life on Mars. An aqueous solution generated by an apparatus like this one can be analyzed by any of a variety of established chromatographic or spectroscopic means to detect the dissolved organic compound(s). The apparatus can be used on Earth: indeed, in proof-of-concept experiments, SCWE was used to extract amino acids from soils of the Atacama Desert (Chile), which was chosen because the dryness and other relevant soil conditions there approximate those on Mars.

The design of the apparatus is based partly on the fact that the relative permittivity (also known as the dielectric constant) of liquid water varies with temperature and pressure. At a temperature of 30 °C and a pressure of 0.1 MPa, the relative permittivity of water is 79.6, due to the strong dipole-dipole electrostatic interactions between individual molecular dipoles. As the temperature increases, increasing thermal energy causes increasing disorientation of molecular dipoles, with a consequent decrease in relative permittivity. For example, water at a temperature of 325 °C and pressure of 20 MPa has a relative permittivity of 17.5, which is similar to the relative permittivities of such nonpolar organic solvents as 1-butanol (17.8). In the operation of this apparatus, the temperature and pressure of water are adjusted so that the water can be used in place of commonly used organic solvents to extract compounds that have dissimilar physical and chemical properties.

Heretofore, laboratory extractions of organic compounds have involved the use, variously, of toxic organic solvents in Soxhlet extraction, strong acids in amino acid vapor-phase hydrolysis, or carbon dioxide as a solvent at supercritical temperature and pressure. Supercritical CO_2 is effective as a solvent for extracting lipids and other very nonpolar organic compounds because its relative permittivity is 1.4 and does not vary significantly with pressure in the range of 7 to 21 MPa or with temperature in the range of 25 to 200 °C. However, supercritical CO_2 is often inadequate as a solvent for extraction of other nonpolar and polar organics. Frequently, it is necessary to mix supercritical CO_2 with methanol or other more-polar organic solvents to obtain an extraction solvent having a greater relative permittivity.

The apparatus (see figure) includes a sample cell, into which a solid sample is

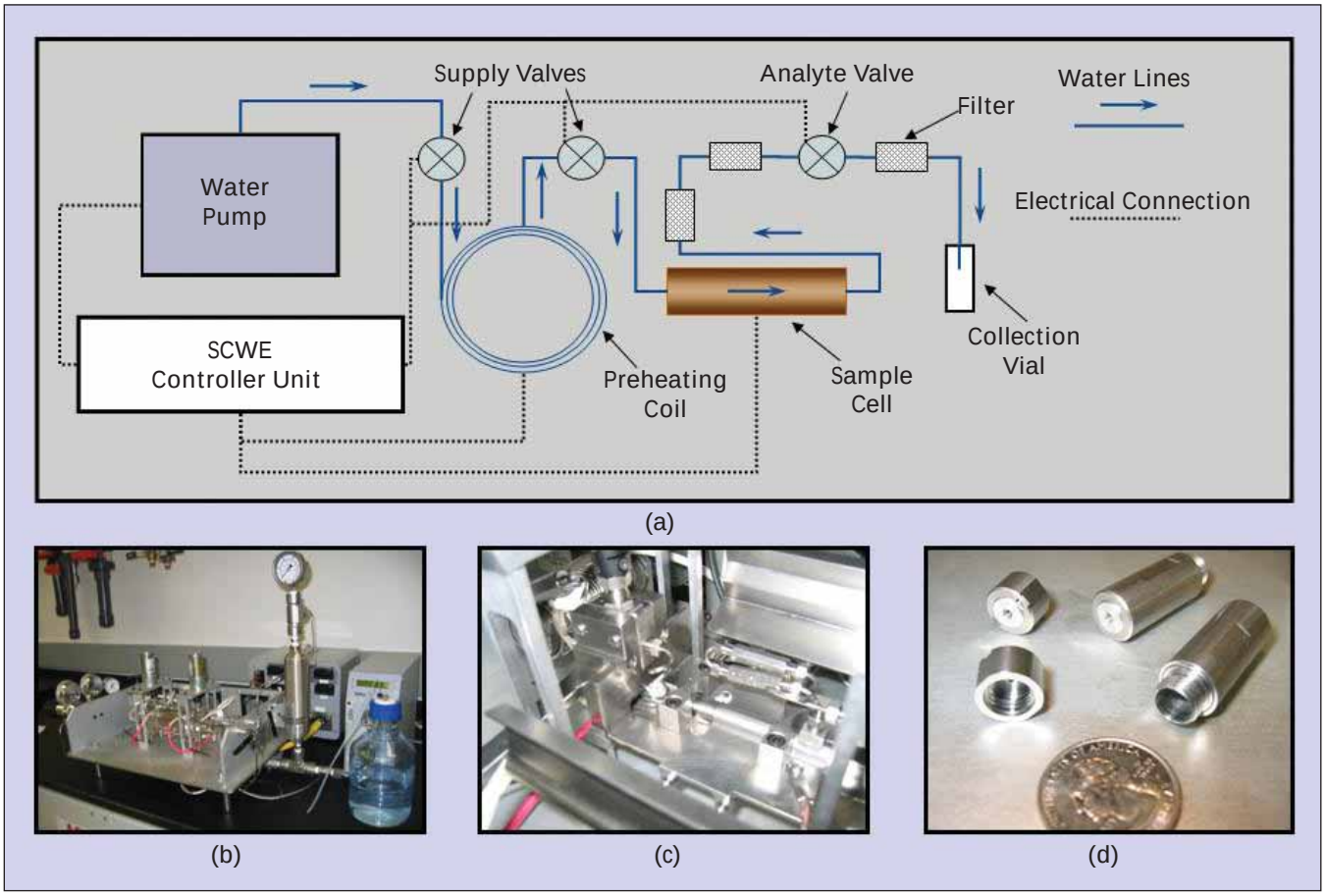

In this **Subcritical-Water Extraction Apparatus**, water at controlled pressure and temperature is pumped through a sample cell that contains a solid matrix material (e.g., a soil) from which organic compounds are to be extracted: (a) SCWE diagram, (b) portable SCWE apparatus, (c) close-up of the sample cell and filtration system, and (d) sample cell.

placed. During a typical extraction, water is pumped to the required high pressure through supply valves, a preheating coil, the sample cell, and an analyte valve into a collection vial. The filters, at various positions downstream of the sample cell, prevent contamination of analytical instruments by particles of the sample solid matrix.

Relative to prior methods and apparatuses used to extract organic compounds, the present apparatus and the method of its operation offer several advantages:

- The solvent (water) is environmentally benign;
- The relative permittivity of the solvent can be adjusted to the values needed to selectively extract, with high efficiency, organic compounds that have different physical and chemical properties;
- The basic principle of operation is simple;
- The apparatus can be highly automated;
- Whereas Soxhlet and hydrolysis extractions often take many hours, an extraction by use of this apparatus takes only minutes.

This work was done by Xenia Amashukeli, Frank Grunthaner, Steven Patrick, James Kirby, Donald Bickler, Peter Willis, Christine Pelletier, and Charles Bryson of Caltech for NASA's Jet Propulsion Laboratory. Further information is contained in a TSP (see page 1).
NPO-44144

A Model for Predicting Thermoelectric Properties of Bi_2Te_3

A compromise between accuracy and computational efficiency is made.

NASA's Jet Propulsion Laboratory, Pasadena, California

A parameterized orthogonal tight-binding mathematical model of the quantum electronic structure of the bismuth telluride molecule has been devised for use in conjunction with a semiclassical transport model in predicting the thermoelectric properties of doped bismuth telluride. This model is expected to be useful in designing and analyzing Bi_2Te_3 thermoelectric devices, including ones that contain such nanostructures as quantum wells and wires. In addition, the understanding gained in the use of this model can be expected to lead to the development of better models that could be useful for developing other thermoelectric materials and devices having enhanced thermoelectric properties.

Bi_2Te_3 is one of the best bulk thermoelectric materials and is widely used in commercial thermoelectric devices. Most prior theoretical studies of the thermoelectric properties of Bi_2Te_3 have involved either continuum models or *ab-initio* models. Continuum models are computationally very efficient, but do not account for atomic-level effects. *Ab-initio* models are atomistic by definition, but do not scale well in that computation times increase excessively with increasing numbers of atoms. The present tight-binding model bridges the gap between the well-scalable but non-atomistic continuum models and the atomistic but poorly scalable *ab-initio* models: The present tight-binding model is atomistic, yet also computationally efficient because of the reduced (relative to an *ab-initio* model) number of basis orbitals and flexible parameterization of the Hamiltonian.

The present tight-binding model includes atomistic descriptions of the Hamiltonian with $sp^3d^5s^*$ basis orbitals, nearest-neighbor interactions, and spin-orbit coupling. For the purposes of the model, within each primitive cell of Bi_2Te_3, two of the Te atoms are denoted Te^I and one is denoted Te^{II}. The difference between Te^I and Te^{II} is that the nearest neighbors of Te^I are three Te atoms and three Bi atoms, while those of Te^{II} are six Bi atoms. To capture the difference, separate tight-binding parameters are assigned to Te^I and Te^{II}.

Altogether, the tight-binding model incorporates 71 independent parameters, which are determined by fitting the computed band structure to a first-principles band structure obtained by use of a submodel based on a screened-exchange local-density approximation. The first-principles band structure predicts the energy gap, the degeneracy of the edges of the conduction and valence bands, and the effective masses of these two bands, in good agreement with experimental results. In the fitting process, a higher priority is given to the highest valence and the lowest conduction bands than to the rest of the band structure, inasmuch as these two bands are mainly responsible for the thermoelectric properties of lightly doped Bi_2Te_3. Moreover, the locations, energies, and effective masses of the two band edges are emphasized, as they largely determine the accuracy of the

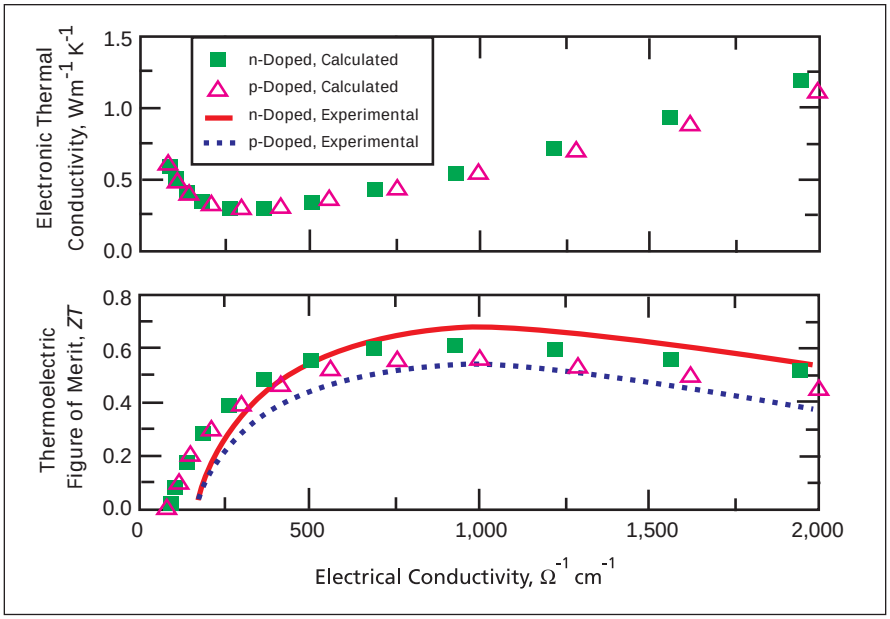

Calculated and Experimental Values of the thermoelectric figure of merit and the electronic thermal conductivity of Bi_2Te_3 were found in fairly close agreement across a broad range of electrical conductivity.

thermoelectric properties predicted by use of this model.

The semiclassical transport model with which this tight-binding model is coupled is a solution of Boltzmann's transport equation in the constant-relaxation-time approximation. The combination of models has been found to yield calculated values of thermoelectric properties within a few percent of experimentally determined values (for example, see figure).

This work was done by Seungwon Lee and Paul Von Allmen of Caltech for NASA's Jet Propulsion Laboratory. For more information, contact iaoffice@jpl.nasa.gov.
NPO-43777

Integrated Miniature Arrays of Optical Biomolecule Detectors

Many biochemical species could be detected simultaneously.

NASA's Jet Propulsion Laboratory, Pasadena, California

Integrated miniature planar arrays of optical sensors for detecting specific biochemicals in extremely small quantities have been proposed. An array of this type would have an area of about 1 cm^2. Each element of the array would include an optical microresonator that would have a high value of the resonance quality factor ($Q \approx 10^7$). The surface of each microresonator would be derivatized to make it bind molecules of a species of interest, and such binding would introduce a measurable change in the optical properties of the microresonator. Because each microresonator could be derivatized for detection of a specific biochemical different from those of the other microresonators, it would be possible to detect multiple specific biochemicals by simultaneous or sequential interrogation of all the elements in the array. Moreover, the derivatization would make it unnecessary to prepare samples by chemical tagging.

Such interrogation would be effected by means of a grid of row and column polymer-based optical waveguides that would be integral parts of a chip on which the array would be fabricated. The row and column polymer-based optical waveguides would intersect at the elements of the array (see figure). At each intersection, the row and column waveguides would be optically coupled to one of the microresonators. The polymer-based waveguides would be connected via optical fibers to external light sources and photodetectors. One set of waveguides and fibers (e.g., the row waveguides and fibers) would couple light from the sources to the resonators; the other set of waveguides and fibers (e.g., the column waveguides and fibers) would couple light from the microresonators to the photodetectors. Each microresonator could be addressed individually by row and column for measurement of its optical transmission. Optionally, the chip could be fabricated so that each microresonator would lie inside a microwell, into which a microscopic liquid sample could be dispensed.

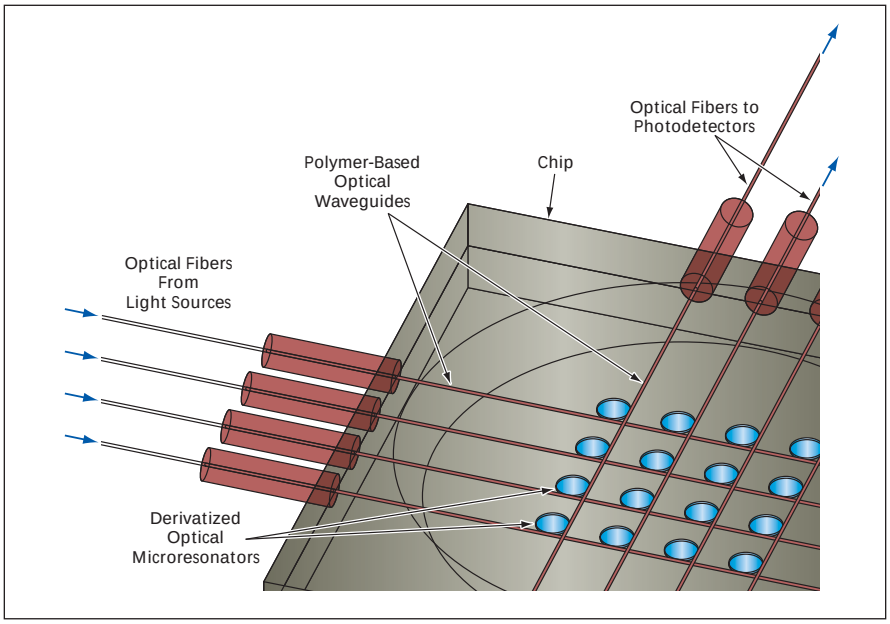

Derivatized Optical Microresonators in an array would address optically via row and column optical waveguides.

This work was done by Vladimir Iltchenko, Lute Maleki, Ying Lin, and Thanh Le of Caltech for NASA's Jet Propulsion Laboratory.

In accordance with Public Law 96-517, the contractor has elected to retain title to this invention. Inquiries concerning rights for its commercial use should be addressed to:

Innovative Technology Assets Management
JPL
Mail Stop 202-233
4800 Oak Grove Drive
Pasadena, CA 91109-8099
E-mail: iaoffice@jpl.nasa.gov

Refer to NPO-43164, volume and number of this NASA Tech Briefs *issue, and the page number.*

A Software Rejuvenation Framework for Distributed Computing

This framework supports graceful degradation of services at best possible performance levels.

NASA's Jet Propulsion Laboratory, Pasadena, California

A performability-oriented conceptual framework for software rejuvenation has been constructed as a means of increasing levels of reliability and performance in distributed stateful computing. As used here, "performability-oriented" signifies that the construction of the framework is guided by the concept of analyzing the ability of a given computing system to deliver services with gracefully degradable performance. The framework is especially intended to support applications that involve stateful replicas of server computers.

Software rejuvenation has been recognized as a simple yet effective means of preventing accumulation of software errors that, if allowed to accumulate, could degrade the capacity or cause failure of a computer system. When a software system is voluntarily rebooted, with high probability, errors accumulated during previous execution are eliminated and the system regains its full capacity. Although software rejuvenation has been investigated extensively, it has not, until now, been considered for stateful applications that involve server replicas. The problem of software rejuvenation in such applications is complicated by the following considerations: When software rejuvenation temporarily stops a long-running replica server, R, the post-rejuvenation performance of R may be reduced because the stoppage may cause the state of R to become inconsistent with the nominal state of other replicas. In that case, R would be unable to provide services at its full capacity until consistency with the states of the other replicas was restored.

The present performability-oriented framework is based on three building blocks: a rejuvenation algorithm, a set of performability metrics, and a performability model. The performability metrics and model both take account of the reduced nature of post-rejuvenation performance pending restoration of consistency. The performability model also takes account of the possibility that post-rejuvenation consistency-restoration processes could be vulnerable to failures because of the potential performance stress caused by service requests accumulated during rejuvenation.

The basic version of the rejuvenation algorithm uses pattern-matching mechanisms to detect pre-failure conditions. To compensate for the inability of pattern-matching mechanisms to detect pre-failure-condition patterns other than those known *a priori*, an enhanced version of the algorithm accommodates a random timer and provides for synergistic coordination of both detection-triggered and timer-triggered rejuvenation. It has been demonstrated, via model-based evaluation, that this performability-oriented framework enables error-accumulation-prone distributed applications to continuously deliver gracefully degradable services at the best possible performance levels, even in environments in which the affected systems are highly vulnerable to failures. It has also been shown that software rejuvenation can be realized as an integral part of the infrastructures in stateful distributed computing applications that guarantee eventual consistency of the states of server replicas.

This work was done by Savio Chau of Caltech for NASA's Jet Propulsion Laboratory.

The software used in this innovation is available for commercial licensing. Please contact Karina Edmonds of the California Institute of Technology at (626) 395-2322. Refer to NPO-42352.

Kurtosis Approach to Solution of a Nonlinear ICA Problem

A gradient-descent algorithm minimizes the kurtosis of an output vector.

NASA's Jet Propulsion Laboratory, Pasadena, California

An algorithm for solving a particular nonlinear independent-component-analysis (ICA) problem, that differs from prior algorithms for solving the same problem, has been devised. The problem in question — of a type known in the art as a post nonlinear mixing problem — is a useful approximation of the problem posed by the mixing and subsequent nonlinear distortion of sensory signals that occur in diverse scientific and engineering instrumentation systems.

Prerequisite for describing this particular post nonlinear ICA problem is a description of the post nonlinear mixing and unmixing models depicted schematically in the figure. The mixing model consists of a linear mixing part followed by a memoryless invertible nonlinear transfer part. The unmixing model consists of a nonlinear inverse transfer part followed by a linear unmixing part. The source signals are recovered if each operation in the unmixing sequence is the inverse of the corresponding operation in the mixing sequence.

More specifically, in the models,

$$\mathbf{s}(n) = [s_1(n), s_2(n), \ldots s_N(n)]^T$$

is an $N \times 1$ column vector representing N independent source signals at time n that one seeks to estimate. This vector is multiplied by $\mathbf{A}$, an initially unknown $N \times N$ matrix that represents the linear mixing of the source signals. The N signals resulting from the mixing are represented by $N \times 1$ column vector

$$\mathbf{v}(n) = [v_1(n), v_2(n), \ldots v_N(n)]^T.$$

Each of these signals is then subjected to nonlinear distortion represented by a function that is initially unknown and could differ from the functions that represent the distortions of the other sig-

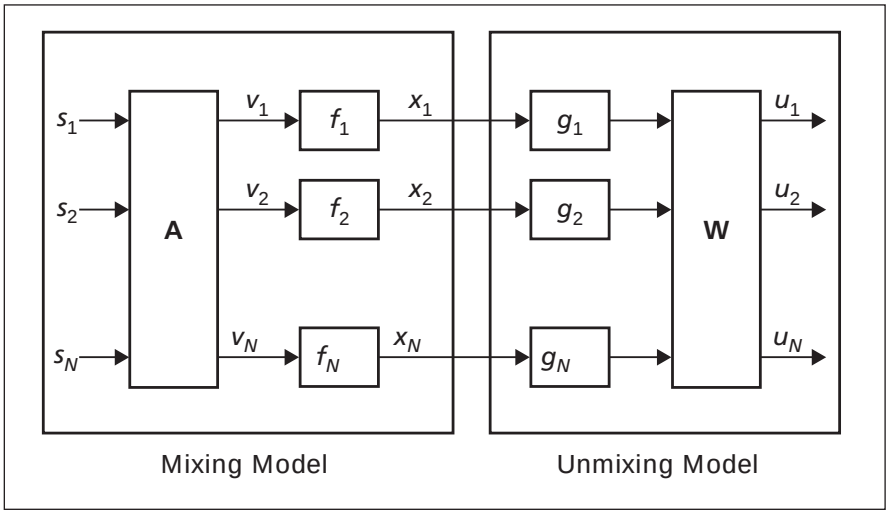

Mixing and Distortion Operations and their inverses are represented in these block-diagram representations of mixing and unmixing models.

nals. For the ith mixture signal, the distorted signal is given by $x_i = f_i(v_i)$, where f_i is one of the initially unknown nonlinear functions. Thus, the vector

$$\mathbf{x}(n) = [x_1(n),x_2(n),...x_N(n)]^T$$

represents instrumentation signals presented for analysis. The distortion in signal x_i is removed by means of a corresponding initially unknown inverse nonlinear function g_i. Finally, the signals are unmixed by means of initially unknown matrix **W** to obtain output vector

$$\mathbf{u}(n) = [u_1(n),u_2(n),...u_N(n)]^T.$$

In the ideal case, **W** would be the inverse of **A** and the output vector **u** would equal the vector, **s**, of source signals.

The particular nonlinear ICA problem is to calculate the nonlinear inverse functions g_i and matrix **W** such that **u** calculated by use of them is a close approximation of **s**. For the purpose of the present algorithm for solving this problem, it is assumed that the inverse nonlinear functions g_i are smooth and can be approximated by polynomials. The algorithm finds the components of the unmixing matrix **W** and the coefficients of the polynomial approximations of g_i by a gradient-descent method. This algorithm utilizes the kurtosis of the components of the output vector **u** as an objective function (in effect, an error measure) that it seeks to minimize. In using the kurtosis, this algorithm stands in contrast to prior algorithms that utilize other objective functions, including statistical functions other than the kurtosis.

This work was done by Vu Duong and Allen Stubberud of Caltech for NASA's Jet Propulsion Laboratory.

In accordance with Public Law 96-517, the contractor has elected to retain title to this invention. Inquiries concerning rights for its commercial use should be addressed to:

Innovative Technology Assets Management
JPL
Mail Stop 202-233
4800 Oak Grove Drive
Pasadena, CA 91109-8099
(818) 354-2240
E-mail: iaoffice@jpl.nasa.gov

Refer to NPO-43088, volume and number of this NASA Tech Briefs issue, *and the page number.*

Robust Software Architecture for Robots

Generalized software can be readily tailored for specific applications.

NASA's Jet Propulsion Laboratory, Pasadena, California

"Robust Real-Time Reconfigurable Robotics Software Architecture" ("R4SA") is the name of both a software architecture and software that embodies the architecture. The architecture was conceived in the spirit of current practice in designing modular, hard, real-time aerospace systems. The architecture facilitates the integration of new sensory, motor, and control software modules into the software of a given robotic system. R4SA was developed for initial application aboard exploratory mobile robots on Mars, but is adaptable to terrestrial robotic systems, real-time embedded computing systems in general, and robotic toys.

The R4SA software, written in clean ANSI C, establishes an onboard, real-time computing environment. The R4SA architecture features three layers: The lowest is the device-driver layer, the highest is the application layer, and the device layer lies at the middle (see figure).

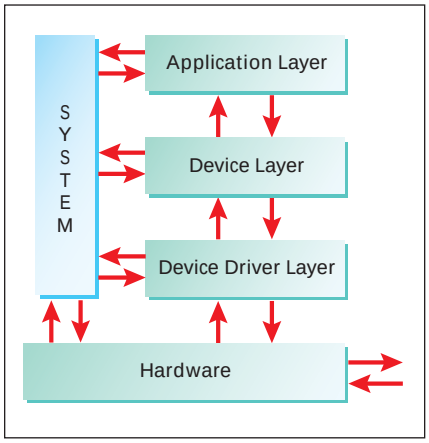

The **R4SA Architecture** features three levels corresponding to different levels of abstraction.

The device-driver layer handles all hardware dependencies. It completely hides the details of how a device works. Activities directed by users are performed by means of well-defined interfaces. Each type of device driver is equipped with its own well-defined interface. For example, the device-driver interface for an analog-to-digital converter differs from that for a digital-to-analog converter.

The device layer provides the means for abstracting the high-level software in the application layer from the hardware dependencies. The device layer provides all motion-control computations, including those for general proportional + integral + derivative controllers, profilers, controllers for such mechanical components as wheels and arms, coordinate-system transformations for odometry and inertial navigation, vision processing, instrument interfaces, communication among multiple robots, and kinematics for a multiple-wheel or multiple-leg robot.

The application layer provides application programs that a robot can execute. Examples of application programs include those needed to perform such prescribed maneuvers as avoiding obstacles while moving from a specified starting point to a specified goal point or turning a robot in place through a specified azimuthal angle. Each robot is provided with application software representing its own unique set of commands. The software establishes a graphical user interface (GUI) for exchanging command information with external computing systems. Via the GUI and its supporting interface software, a user can select and assemble, from the aforementioned set, commands appropriate to the task at hand and send the commands to the robot for execution. System software that interacts with the R4SA software at all three levels establishes a synchronized control environment.

The R4SA software features two modes of execution: before real time (BRT) and real time (RT). In the BRT mode, a text configuration file is read in (each robot has its own unique file) and then device-driver-layer, device-layer, and application-layer initialization functions are executed. If execution is successful, then the system jumps into the RT mode, in which the system is ready to receive and execute commands.

One goal in developing the R4SA architecture was to provide one computer code for many robots. The unique executable code for each robot is built by use of a configuration feature file. The set of features for a given robot is selected from a feature database on the basis of the hardware and mechanical capabilities of that robot. Recompilation of code is straightforward: modifications can readily be performed in the field by use of simple laptop-computer development and debugging software tools.

This work was done by Hrand Aghazarian, Eric Baumgartner, and Michael Garrett of Caltech for NASA's Jet Propulsion Laboratory. Further information is contained in a TSP (see page 1).

The software used in this innovation is available for commercial licensing. Please contact Karina Edmonds of the California Institute of Technology at (626) 395-2322. Refer to NPO-41796.

R4SA for Controlling Robots

NASA's Jet Propulsion Laboratory, Pasadena, California

The R4SA GUI mentioned in the immediately preceding article is a user-friendly interface for controlling one or more robot(s). This GUI makes it possible to perform meaningful real-time field experiments and research in robotics at an unmatched level of fidelity, within minutes of setup. It provides such powerful graphing modes as that of a digitizing oscilloscope that displays up to 250 variables at rates between 1 and 200 Hz. This GUI can be configured as multiple intuitive interfaces for acquisition of data, command, and control to enable rapid testing of subsystems or an entire robot system while simultaneously performing analysis of data.

The R4SA software establishes an intuitive component-based design environment that can be easily reconfigured for any robotic platform by creating or editing setup configuration files. The R4SA GUI enables event-driven and conditional sequencing similar to those of Mars Exploration Rover (MER) operations. It has been certified as part of the MER ground support equipment and, therefore, is allowed to be utilized in conjunction with MER flight hardware. The R4SA GUI could also be adapted to use in embedded computing systems, other than that of the MER, for commanding and real-time analysis of data.

This work was done by Hrand Aghazarian of Caltech for NASA's Jet Propulsion Laboratory. Further information is contained in a TSP (see page 1).

The software used in this innovation is available for commercial licensing. Please contact Karina Edmonds of the California Institute of Technology at (626) 395-2322. Refer to NPO-41797.

Bio-Inspired Neural Model for Learning Dynamic Models

This model could be a basis for fast speech- and image-recognition computers.

NASA's Jet Propulsion Laboratory, Pasadena, California

A neural-network mathematical model that, relative to prior such models, places greater emphasis on some of the temporal aspects of real neural physical processes, has been proposed as a basis for massively parallel, distributed algorithms that learn dynamic models of possibly complex external processes by means of learning rules that are local in space and time. The algorithms could be made to perform such functions as recognition and prediction of words in speech and of objects depicted in video images. The approach embodied in this model is said to be "hardware-friendly" in the following sense: The algorithms would be amenable to execution by special-purpose computers implemented as very-large-scale integrated (VLSI) circuits that would operate at relatively high speeds and low power demands.

It is necessary to present a large amount of background information to give meaning to a brief summary of the present neural-network model:

- A dynamic model to be learned by the present neural-network model is of a type denoted an internal model or predictor. In simplest terms, an internal model is a set of equations that predicts future measurements on the basis of past and current ones. Internal models have been used in controlling industrial plants and machines (including robots).
- One of the conclusions drawn from Pavlov's famous experiments was the observation that reinforcers of learning (basically, rewards and punishments) become progressively less efficient for causing adaptation of

behavior as their predictability grows during the course of learning. The difference between the actual occurrence and the prediction of the reinforcer is denoted as the reinforcement prediction error signal. In what is known in the art as the temporal-difference model (TD model) of Pavlovian learning, the reinforcement prediction error signal is used to learn a reinforcement prediction signal. The desired reinforcement prediction signal is defined as a weighted sum of future reinforcement signals wherein reinforcements are progressively discounted with increasing time into the future. The reinforcement prediction error signal progressively decreases during learning as the reinforcement prediction signal becomes more similar to the desired reinforcement prediction signal.

- Algorithms based on the TD model ("TD algorithms") have been analyzed and shown to be implementations of a variant of dynamic programming. Machine-learning studies have shown that TD algorithms are powerful means of solving reinforcement learning problems that involve delayed reinforcement. Examples of such problems include board games, which involve delayed rewards (winning) or punishments (losing).
- Mid-brain dopamine neurons are so named because they modulate the levels of activity of other neurons by means of the neurotransmitter chemical dopamine. The cell bodies of dopamine neurons are located in the brain stem and their axons project to many brain areas. Activities of dopamine neurons have been found to be strikingly similar to the prediction error signals of the TD model.
- Real neural signals include spikelike pulses, the times of occurrence of which are significant. The term "biological spike coding" denotes, essentially, temporal labeling of such pulses in real neurons or in a neural-network model.

This concludes the background information.

The present neural-network model incorporates biological spike coding along with some basic principles of the learning by synapses in the cortex of the human brain. According to the learning rule of the model, synaptic weights are adapted when pre- and postsynaptic spikes occur within short time windows. In simplified terms, for a given synapse and time window, the synaptic strength is increased in the long term if the presynaptic spike precedes the postsynaptic spike or is decreased in the long term if the presynaptic spike follows the postsynaptic spike. This learning rule has been shown to minimize prediction errors, indicating that the neural network learns an optimal dynamic model of an external process.

This work was done by Tuan Duong, Vu Duong, and Roland Suri of Caltech for NASA's Jet Propulsion Laboratory.

In accordance with Public Law 96-517, the contractor has elected to retain title to this invention. Inquiries concerning rights for its commercial use should be addressed to:

Innovative Technology Assets Management
JPL
Mail Stop 202-233
4800 Oak Grove Drive
Pasadena, CA 91109-8099
(818) 354-2240
E-mail: iaoffice@jpl.nasa.gov

Refer to NPO-41691, volume and number of this NASA Tech Briefs *issue, and the page number.*

Evolutionary Computing Methods for Spectral Retrieval

Solutions to the inverse problem of spectral retrieval are found in a computationally efficient process.

NASA's Jet Propulsion Laboratory, Pasadena, California

A methodology for processing spectral images to retrieve information on underlying physical, chemical, and/or biological phenomena is based on evolutionary and related computational methods implemented in software. In a typical case, the solution (the information that one seeks to retrieve) consists of parameters of a mathematical model that represents one or more of the phenomena of interest.

The methodology was developed for the initial purpose of retrieving the desired information from spectral image data acquired by remote-sensing instruments aimed at planets (including the Earth). Examples of information desired in such applications include trace gas concentrations, temperature profiles, surface types, day/night fractions, cloud/aerosol fractions, seasons, and viewing angles. The methodology is also potentially useful for retrieving information on chemical and/or biological hazards in terrestrial settings.

In this methodology, one utilizes an iterative process that minimizes a fitness function indicative of the degree of dissimilarity between observed and synthetic spectral and angular data. The evolutionary computing methods that lie at the heart of this process yield a population of solutions (sets of the desired parameters) within an accuracy represented by a fitness-function value specified by the user. The evolutionary computing methods (ECM) used in this methodology are Genetic Algorithms and Simulated Annealing, both of which are well-established optimization techniques and have also been described in previous *NASA Tech Briefs* articles. These are embedded in a conceptual framework, represented in the architecture of the implementing software, that enables automatic retrieval of spectral and angular data and analysis of the retrieved solutions for uniqueness. This framework is composed of three modules (see figure):

1. The central core, which consists of the aforementioned ECM;
2. The synthetic-spectra generator, which, coupled with the ECM, generates a population of automatically retrieved spectral solutions; and
3. The synthetic-spectra degeneracy analyzer ("degeneracy" is used here in the mathematical sense of signifying the existence of multiple equally valid solutions for a given set of data and user-defined accuracy), which applies several well-established mathematical methods to characterize the uniqueness (or the degeneracy, which is essentially the lack of uniqueness) of the solutions within the population.

One advantage afforded by this ECM-based methodology over traditional spectral retrieval methods is the ability to perform an automatic, unbiased search for all solutions within the entire parameter

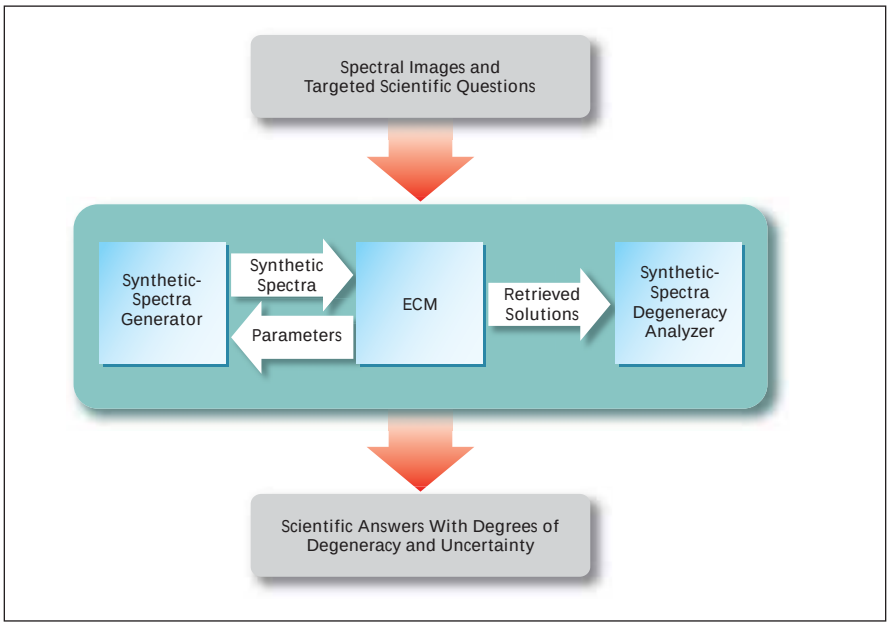

This **Conceptual Framework for Spectral Retrieval**, and the software that implements it, comprises three modules that interact in an iterative process.

space, using criteria that make searching computationally far more economical than in complete-enumeration ("brute force"), Monte Carlo, or random searches. (As used here, "unbiased" characterizes a search that does not depend on initial *ad hoc* guesses by experts.) Other advantages include the following:

- Optimal solutions are found;
- Better interpretations of planetary spectral and angular data are possible, and initial tests have shown these interpretations to be consistent with ground truth; and
- The methodology is not limited to specific problems, and can be extended to solve problems of greater complexity.

This work was done by Richard Terrile, Wolfgang Fink, Terrance Huntsberger, Seungwon Lee, Edwin Tisdale, Paul Von Allmen, and Giovanna Tinetti of Caltech for NASA's Jet Propulsion Laboratory. Further information is contained in a TSP (see page 1).

In accordance with Public Law 96-517, the contractor has elected to retain title to this invention. Inquiries concerning rights for its commercial use should be addressed to:

Innovative Technology Assets Management
JPL
Mail Stop 202-233
4800 Oak Grove Drive
Pasadena, CA 91109-8099
(818) 354-2240
E-mail: iaoffice@jpl.nasa.gov

Refer to NPO-42564, volume and number of this NASA Tech Briefs *issue, and the page number.*

Monitoring Disasters by Use of Instrumented Robotic Aircraft

Real-time synoptic data would help in coordinating and planning responses.

Ames Research Center, Moffett Field, California

Efforts are under way to develop data-acquisition, data-processing, and data-communication systems for monitoring disasters over large geographic areas by use of uninhabited aerial systems (UAS) — robotic aircraft that are typically piloted by remote control. As integral parts of advanced, comprehensive disaster-management programs, these systems would provide (1) real-time data that would be used to coordinate responses to current disasters and (2) recorded data that would be used to model disasters for the purpose of mitigating the effects of future disasters and planning responses to them.

The basic idea is to equip UAS with sensors (e.g., conventional video cameras and/or multispectral imaging instruments) and to fly them over disaster areas, where they could transmit data by radio to command centers. Transmission could occur along direct line-of-sight paths and/or along over-the-horizon paths by relay via spacecraft in orbit around the Earth. The initial focus is on demonstrating systems for monitoring wildfires; other disasters to which these developments are expected to be applicable include floods, hurricanes, tornadoes, earthquakes, volcanic eruptions, leaks of toxic chemicals, and military attacks.

The figure depicts a typical system for monitoring a wildfire. In this case, instruments aboard a UAS would generate calibrated thermal-infrared digital image data of terrain affected by a wildfire. The data would be sent by radio via satellite to a data-archive server and image-processing computers. In the image-processing computers, the data would be rapidly geo-rectified for processing by one or more of a large variety of geographic-information-system (GIS) and/or image-analysis software packages. After processing by this software, the data would be both stored in the archive and distributed through standard Internet connections to a disaster-mitigation center, an investigator, and/or command center at the scene of the fire.

Ground assets (in this case, firefighters and/or firefighting equipment) would also be monitored in real time by use of Global Positioning System (GPS) units and radio communication links between the assets and the UAS. In this scenario, the UAS would serve as a data-relay station in the sky, sending packets of information concerning the locations of assets to the image-processing computer, wherein this information would be incorporated into the geo-rectified images and maps. Hence, the images and maps would enable command-center personnel to monitor locations of assets in real time and in relation to locations affected by the disaster. Optionally, in case of a disaster that disrupted communications, the UAS could be used as an airborne communication relay station to partly restore communications to the affected area.

A prototype of a system of this type was demonstrated in a project denoted the First Response Experiment (Project FiRE). In this project, a controlled outdoor fire was observed by use of a thermal multispectral scanning imager on a

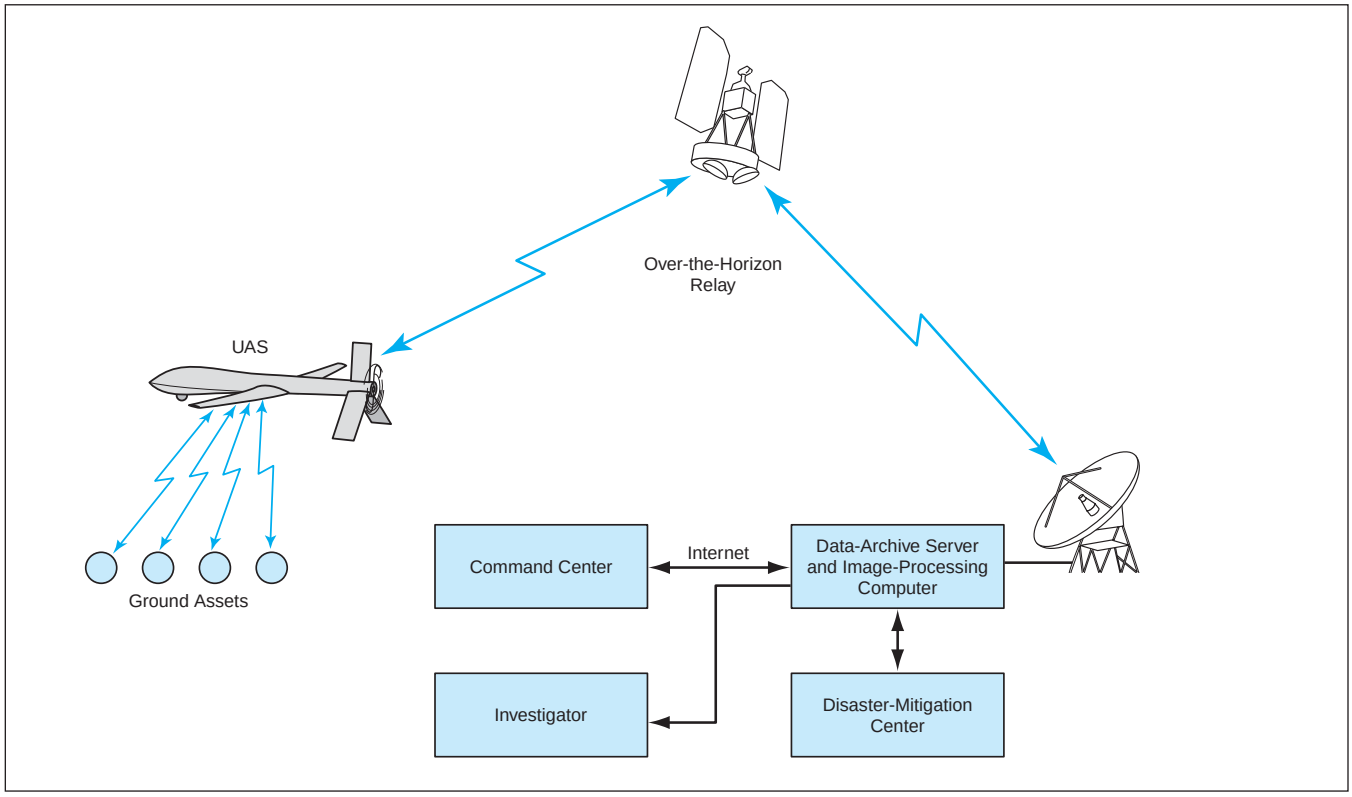

Monitoring by Instruments Aboard a UAS would provide information to coordinate actions of ground assets at the scene of a disaster. The UAS and one or more satellite(s) would also serve as communication relays.

UAS that delivered image data to a ground station via a satellite uplink/downlink telemetry system. At the ground station, the image data were georectified in nearly real time for distribution via the Internet to firefighting managers. Project FiRE was deemed a success in demonstrating several advances essential to the eventual success of the continuing development effort.

This work was done by Steven S. Wegener, Donald V. Sullivan, Steven E. Dunagan, and James A. Brass of Ames Research Center; Vincent G. Ambrosia of California State University — Monterey Bay; Sally W. Buechel of Terra-Mar Resource Information Services; Jay Stoneburner of General Atomics-Aeronautical Systems, Inc.; and Susan M. Schoenung of Longitude 122 West, Inc. For further information, access http://geo.arc.nasa.gov/sge/UAVFiRE/whitepaper.html or contact the Ames Technology Partnerships Division at (650) 604-2954. ARC-14999-1.

Complexity for Survival of Living Systems

Interactions between systems and their mental images enable unlimited increase of complexity.

NASA's Jet Propulsion Laboratory, Pasadena, California

A logical connection between the survivability of living systems and the complexity of their behavior (equivalently, mental complexity) has been established. This connection is an important intermediate result of continuing research on mathematical models that could constitute a unified representation of the evolution of both living and non-living systems. Earlier results of this research were reported in several prior *NASA Tech Briefs* articles, the two most relevant being "Characteristics of Dynamics of Intelligent Systems" (NPO-21037), *NASA Tech Briefs*, Vol. 26, No. 12 (December 2002), page 48; and "Self-Supervised Dynamical Systems" (NPO-30634) *NASA Tech Briefs*, Vol. 27, No. 3 (March 2003), page 72.

As used here, "living systems" is synonymous with "active systems" and "intelligent systems." The quoted terms can signify artificial agents (e.g., suitably programmed computers) or natural biological systems ranging from single-cell organisms at one extreme to the whole of human society at the other extreme. One of the requirements that must be satisfied in mathematical modeling of living systems is reconciliation of evolution of life with the second law of thermodynamics. In the approach followed in this research, this reconciliation is effected by means of a model, inspired partly by quantum mechanics, in which the quantum potential is replaced with an information potential. The model captures the most fundamental property of life — the ability to evolve from disorder to order without any external interference.

The model incorporates the equations of classical dynamics, including Newton's equations of motion and equations for random components caused by uncertainties in initial conditions and by Langevin forces. The equations of classical dynamics are coupled with corresponding Liouville or Fokker-Planck

equations that describe the evolutions of probability densities that represent the uncertainties. The coupling is effected by fictitious information-based forces that are gradients of the information potential, which, in turn, is a function of the probability densities. The probability densities are associated with mental images — both self-image and nonself images (images of external objects that can include other agents). The evolution of the probability densities represents mental dynamics. Then the interaction between the physical and metal aspects of behavior is implemented by feedback from mental to motor dynamics, as represented by the aforementioned fictitious forces.

The interaction of a system with its self and nonself images affords unlimited capacity for increase of complexity. There is a biological basis for this model of mental dynamics in the discovery of mirror neurons that learn by imitation. The levels of complexity attained by use of this model match those observed in living systems. To establish a mechanism for increasing the complexity of dynamics of an active system, the model enables exploitation of a chain of reflections exemplified by questions of the form, "What do you think that I think that you think...?" Mathematically, each level of reflection is represented in the form of an attractor performing the corresponding level of abstraction with more details removed from higher levels. The model can be used to describe the behaviors, not only of biological systems, but also of ecological, social, and economics ones. a

This work was done by Michail Zak of Caltech for NASA's Jet Propulsion Laboratory. For more information contact iaoffice@jpl.nasa.gov.
NPO-43302

Books & Reports

Using Drained Spacecraft Propellant Tanks for Habitation

A document proposes that future spacecraft for planetary and space exploration be designed to enable reuse of drained propellant tanks for occupancy by humans. This proposal would enable utilization of volume and mass that would otherwise be unavailable and, in some cases, discarded. Such utilization could enable reductions in cost, initial launch mass, and number of launches needed to build up a habitable outpost in orbit about, or on the surface of, a planet or moon. According to the proposal, the large propellant tanks of a spacecraft would be configured to enable crews to gain access to their interiors.

The spacecraft would incorporate hatchways, between a tank and the crew volume, that would remain sealed while the tank contained propellant and could be opened after the tank was purged by venting to outer space and then refilled with air. The interior of the tank would be pre-fitted with some habitation fixtures that were compatible with the propellant environment. Electrical feedthroughs, used originally for gauging propellants, could be reused to supply electric power to equipment installed in the newly occupied space. After a small amount of work, the tank would be ready for long-term use as a habitation module.

This work was done by Andrew S. W. Thomas of Johnson Space Center. Further information is contained in a TSP (see page 1).
MSC-24236-1

Connecting Node

A paper describes the Octanode, a connecting node that facilitates the integration of multiple docking mechanisms, hatches, windows, and internal and external systems with the use of flat surfaces. The Octanode is a 26-faced Great Rhombicuboctahedron Archimedean solid with six octagon-shaped panels, eight hexagon-shaped panels, and 12 square panels using three unique, simple, flat shapes to construct a spherical approximation. Each flat shape can be constructed with a variety of material and manufacturing techniques, such as honeycomb composite panels or a pocketed skin-stringer configuration, using conventional means.

The flat shapes can be connected together and sealed to create a pressurizable volume by the use of any conventional means including welding or fastening devices and sealant. The node can then be connected to other elements to allow transfer between those elements, or it could serve as an airlock. The Octanode can be manufactured on the ground and can be integrated with subsystems including hatches and ports. The node can then be transported to its intended location, whether on orbit or on surface. Any of the flat panels could be replaced by curved ones, turning the node into a copula.

Windows may be placed on flat panes with optimal viewing angles that are not blocked by large connecting nodes. The advantage of using flat panels to represent a spherical approximation is that this allows for easier integration of subsystems and design features.

This work was done by Christopher J. Johnson, Jasen L. Raboin, and Gary R. Spexarth for Johnson Space Center. Further information is contained in a TSP (see page 1).

This invention is owned by NASA, and a patent application has been filed. Inquiries concerning nonexclusive or exclusive license for its commercial development should be addressed to the Patent Counsel, Johnson Space Center, (281) 483-1003. Refer to MSC-24216-1.

Electrolytes for Low-Temperature Operation of Li-CF_x Cells

A report describes a study of electrolyte compositions selected as candidates for improving the low-temperature performances of primary electrochemical cells that contain lithium anodes and fluorinated carbonaceous (CF_x) cathodes. This study complements the developments reported in "Additive for Low-Temperature Operation of Li-$(CF)_n$ Cells" (NPO-43579) and Li/CF_x Cells Optimized for Low-Temperature Operation (NPO-43585), which appear elsewhere in this issue of *NASA Tech Briefs*.

Similar to lithium-based electrolytes described in several previous *NASA Tech Briefs* articles, each of these electrolytes consisted of a lithium salt dissolved in a nonaqueous solvent mixture. Each such mixture consisted of two or more of the following ingredients: propylene carbonate (PC); 1,2-dimethoxyethane (DME); trifluoropropylene carbonate; *bis*(2,2,2-trifluoroethyl) ether; diethyl carbonate; dimethyl carbonate; and ethyl methyl carbonate. The report describes the physical and chemical principles underlying the selection of the compositions (which were not optimized) and presents results of preliminary tests made to determine effects of the compositions upon the low-temperature capabilities of Li-CF_x cells, relative to a baseline composition of $LiBF_4$ at a concentration of 1.0 M in a solvent comprising equal volume parts of PC and DME.

This work was done by Marshall C. Smart, Jay F. Whitacre, and Ratnakumar V. Bugga of Caltech; and G. K. Surya Prakash, Pooja Bhalla, and Kiah Smith of the Loker Hydrocarbon Institute at the University of Southern California for NASA's Jet Propulsion Laboratory. Further information is contained in a TSP (see page 1).

In accordance with Public Law 96-517, the contractor has elected to retain title to this invention. Inquiries concerning rights for its commercial use should be addressed to:

Innovative Technology Assets Management
JPL
Mail Stop 202-233
4800 Oak Grove Drive
Pasadena, CA 91109-8099
(818) 354-2240
E-mail: iaoffice@jpl.nasa.gov

Refer to NPO-43587, volume and number of this NASA Tech Briefs *issue, and the page number.*


NASA
National Aeronautics and
Space Administration